An experimental and kinetic modeling study of phenylacetylene decomposition and the reactions with acetylene/ethylene under shock tube pyrolysis conditions

Wenyu Sun, Alaa Hamadi, Said Abid, Nabiha Chaumeix, Andrea Comandini

Combustion and Flame 220 (2020) 257–271

Contents lists available at ScienceDirect

Combustion and Flame

journal homepage: www.elsevier.com/locate/combustflame

An experimental and kinetic modeling study of phenylacetylene decomposition and the reactions with acetylene/ethylene under shock tube pyrolysis conditions

Wenyu Sun[a,*], Alaa Hamadi[a], Said Abid[a,b], Nabiha Chaumeix[a], Andrea Comandini[a,*]

[a] CNRS-INSIS, I.C.A.R.E., 1C, Avenue de la recherche scientifique, 45071 Orléans cedex 2, France
[b] Université d'Orléans, 6 Avenue du Parc Floral, 45100 Orléans, France

ARTICLE INFO

Article history:
Received 3 February 2020
Revised 29 June 2020
Accepted 30 June 2020
Available online 16 July 2020

Keywords:
Phenylacetylene
Acetylene
Ethylene
Single-pulse shock tube
Polycyclic aromatic hydrocarbons (PAHs)

ABSTRACT

Pyrolysis of phenylacetylene with and without the presence of C_2 hydrocarbons (acetylene or ethylene) was studied in a single-pulse shock tube coupled to gas chromatography/gas chromatography-mass spectrometry equipment for speciation diagnostics. Quantitative speciation profiles were probed from each reaction system over the temperature range of 1100–1700 K at a nominal pressure of 20 bar. A kinetic model was proposed to interpret how phenylacetylene is consumed under high-pressure pyrolytic conditions and how the resulting intermediates react to form polycyclic aromatic hydrocarbons (PAHs), and furthermore, how the extra acetylene or ethylene alter the reaction schemes. It was found that the bimolecular reaction between phenylacetylene and hydrogen atom leading to phenyl and acetylene dominates phenylacetylene decomposition throughout the temperature window. The addition/elimination reactions between phenylacetylene and phenyl not only produce hydrogen atoms to maintain the reactivity of the fuel decay, but also directly lead to the formation of several $C_{14}H_{10}$ PAH isomers including diphenylacetylene, 9-methylene-fluorene and phenanthrene. Intermediates pools, regarding both species categories and abundance, are changed by the two C_2 fuels introduced into the reaction system. The added acetylene enables the Hydrogen-Abstraction-Acetylene-Addition (HACA) mechanism starting from the phenylacetylene radical to occur at relatively low temperatures. But the yielded naphthyl core does not stabilize in naphthalene due to the lack of hydrogen atoms in the reaction system, and instead, it carries on the HACA route by further combining with another acetylene molecule, ending up in acenaphthylene. Differently, the added ethylene intensifies the HACA routes by contributing to the acetylene formation, and more importantly, provides hydrogen atoms participating in the naphthalene formation from naphthyl radical.

1. Introduction

An in-depth understanding of polycyclic aromatic hydrocarbons (PAHs) formation mechanisms would benefit the numerical designs of advanced clean combustion devices. Detailed kinetic models of PAH formation in combustion have been under development for decades [1–3], resulting in an improved understanding of mechanistic pathways and an increasing refinement of the parameters describing the temperature and pressure dependence of important reactions. Among the reaction schemes postulated for PAH formation, the Hydrogen-Abstraction-Carbon-Addition (HACA) routes [4–7] are the best known and the most studied; the general multistep process proceeds by abstraction of a hydrogen atom from an aromatic ring, creating a phenyl-type radical that subsequently adds to C_2H_2 and ultimately undergoes ring-closure to increase the size of the PAH. As shown in Scheme 1, phenylacetylene ($C_6H_5C_2H$) is an essential intermediate on the HACA pathway of naphthyl formation from benzene, which is representative of aromatic growth processes. Important reactions, such as the formation of $C_6H_5C_2H$ from phenyl (C_6H_5) [6,8–11], the C_2H_2 addition to the *ortho*-radical ($C_6H_4C_2H$) of $C_6H_5C_2H$ resulting in a naphthyl core [6,9], attracted considerable research attention.

The fate of $C_6H_5C_2H$, including the pathways leading to $C_6H_4C_2H$ formation as well as other competing channels, could impact the effectiveness of the HACA routes. However, due to a lack of pertinent studies, the consumption scheme of $C_6H_5C_2H$ under

* Corresponding authors.
E-mail addresses: wenyu.sun@cnrs-orleans.fr (W. Sun), andrea.comandini@cnrs-orleans.fr (A. Comandini).

https://doi.org/10.1016/j.combustflame.2020.06.044

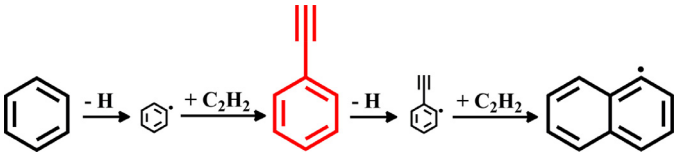

Scheme 1. Schematic of the HACA mechanism of naphthyl formation from benzene.

combustion relevant conditions is not yet well established. To the best of our knowledge, the only available kinetic investigation centering on $C_6H_5C_2H$ consumption is the shock tube study by Herzler and Frank [12], in which rate coefficients for major reactions accounting for $C_6H_5C_2H$ decomposition were derived at a pressure of around 2 bar over the temperature range of 1600–1900 K. It is not uncommon that in existing combustion kinetic models for aromatic fuels [2,13–16], sub-mechanisms of $C_6H_5C_2H$ were constructed through analogies to reactions of other mono-ring aromatics such as benzene, toluene or even styrene, whose consumption schemes are better investigated. Such sub-mechanisms, despite their kinetic significance, are not well validated, owing to a scarcity of experimental data on the fate of $C_6H_5C_2H$.

In practical combustion processes of aliphatic hydrocarbons, acetylene (C_2H_2) and ethylene (C_2H_4) are produced in large amounts. Their interactions with aromatic molecules or radicals in the species pools are recognized as crucial in the build-up of PAH compounds. To address relevant pathways from the fundamental experimental point of view, previous investigators introduced unsaturated C_2H_x compounds to pyrolysis and flame systems of small aromatics, such as benzene [17–20], phenyl [21], toluene [22,23], to monitor their effects on PAH or soot formation. The essential interactions between $C_6H_5C_2H$ and C_2H_2, which could directly lead to the formation of the naphthalene core, however, have never been directly examined through experimental methods.

Inspired by the above, one major task in the present work is to understand the speciation behaviors related to PAH formation from $C_6H_5C_2H$ decomposition. A second goal is to understand how the resulting species pool reacts with C_2H_2 and C_2H_4. Recent studies [24,25] suggested that the combustion processes can be decoupled into separate pyrolysis and oxidation steps. Therefore, we chose to unravel the mentioned issues under high-pressure pyrolysis conditions where specific pathways can be focused with reduced kinetic complexity. Towards these goals, shock tube pyrolysis experiments for $C_6H_5C_2H$, as well as $C_6H_5C_2H$+C_2H_x blends are carried out under identical conditions. In the blended mixtures, more than half of the carbon is supplied by C_2H_2 or C_2H_4 to better highlight the effects of C_2H_x. Speciation information is obtained from each case through gas chromatography/gas chromatography-mass spectrometry (GC/GC–MS) measurements. The different species pools brought by the initial fuel compositions are compared among the three cases. A kinetic model is also proposed, not only to interpret $C_6H_5C_2H$ consumption, but also to account for the interactions between $C_6H_5C_2H$ and C_2H_x under high-pressure pyrolysis conditions. Crucial reaction channels and their roles at different temperatures are highlighted.

2. Shock tube pyrolysis experiments

The pyrolysis experiments in this work were carried out at the single-pulse shock tube facility of ICARE, CNRS, Orléans, France. Descriptions and a schematic of the experimental set-up are detailed in our recent work [26]. The driven section of the shock tube, with an inner diameter of 78 mm and a length of 6 m, is separated from the driver section (120 mm in inner diameter and 3.7 m in length) by a double diaphragm. A dump tank with the volume of 150 L is placed close the diaphragm on the driven section side to operate the shock tube in the single-pulsed fashion. A series of four pressure sensors (CHIMIE METAL A25L05B) are mounted at intervals of 150 mm near the end of the driven section, with the last one being 82 mm away from the endwall. The pressure signals are used to calculate the velocity of the incident shock wave, which is subsequently used to determine the temperature and pressure conditions (T_5 and P_5) behind the reflected shock wave by solving conservation equations together with the ideal gas law and variable heat capacity ratio. In particular, an iterative method is used to derive T_2 starting from the initial state of the testing mixture (P_1 and T_1) till the convergence is reached, *i.e.*, when the difference between the calculated and measured incident shock velocity is less than 10^{-6} m/s; P_2 is then derived from the ideal gas law. A similar procedure is implemented to derive T_5 and P_5 and the convergence criterion in solving the shock wave equations is that the absolute value of $U_2{}^*(1\text{-}\rho_2/\rho_1)\text{-}U_5{}^*(1\text{-}\rho_5/\rho_2)$ reaches below10^{-6} m/s. No difference is observed between the results computed with the above-mentioned method and those obtained using relevant commercial codes. The estimated errors introduced by the solution of the conservation equations and the use of the ideal gas law are small, compared to those derived from the uncertainties in incident shock wave velocities. Indeed, the uncertainty in the calculated T_5, which mainly comes from the errors in the actual positions of the pressure sensors, is within ±30 K. A PCB pressure sensor shielded by a layer of room-temperature vulcanizing (RTV) silicone is located on the end-wall to record the endwall pressure history. The reaction time for each operation is defined with the pressure trace as the time interval between the arrival of the shock wave and the point when the pressure drops to 80% P_5 [26]. The reaction time with the current experimental configuration is around 4.0 ms. An air-actuated HIP valve is mounted on the endwall center to sample the post-shock gas mixtures in which the reactions are quenched by the cooling rarefaction waves. The operation of the sampling valve is triggered by the PCB pressure signal by setting a delay of 4.0 ms (equal to the nominal reaction time), while the opening and closing of the valve takes hundreds of milliseconds, due to mechanical constrains. The alternative use of fast micro-size valves, which are capable to operate within a few milliseconds, was tested by other research groups [27]: it would reduce the sample volumes withdrawn from the shock tube, and consequently, the sensitivity of GC analyses, making it impossible to measure PAHs at the sub-ppm level. Approximately 20 ml gas (at an equivalent pressure of about 1.5 bar) is withdrawn each time to the transfer line downstream. Given the relatively large volume of the sampled gas and the slow sampling, the average velocity of the incident shock wave, instead of the extrapolated value at the endwall, is used in to calculate P_5 and T_5 in this work to better characterize the actual conditions encountered by the gas samples. The transfer line is made up of SilcoTek tubes heated at 150 °C to the analytical equipment consisting of two GCs placed in series. The gas sample is injected into the GC column when the pressure in the line is stabilized (usually taking a few seconds), and the injection pressure is recorded to normalize GC signals for quantification. The first GC (Agilent 7890) is equipped with a flame ionization detector (FID) connected to a DB-17-ms column for heavy species separation (250 µl sample loop, splitless mode), and a thermal conductivity detector (TCD) coupled to a Molsieve 5A column to monitor the absence of air and the dilution coming from helium in the driver section (1 ml sample loop, splitless mode). The valves of this GC are placed in an external oven, which could regulate the temperature up to 300 °C, to avoid condensation of heavy species in the sample. The second GC (Thermo Trace GC Ultra) is equipped with an FID connected to an HP Plot Q column to measure light species up to mono-aromatics (1 ml sample loop, split mode); a DSQ mass spectrometer is also incorporated to aid in the species identification which is mainly based on the retention time of different PAHs known from prior injections of standards.

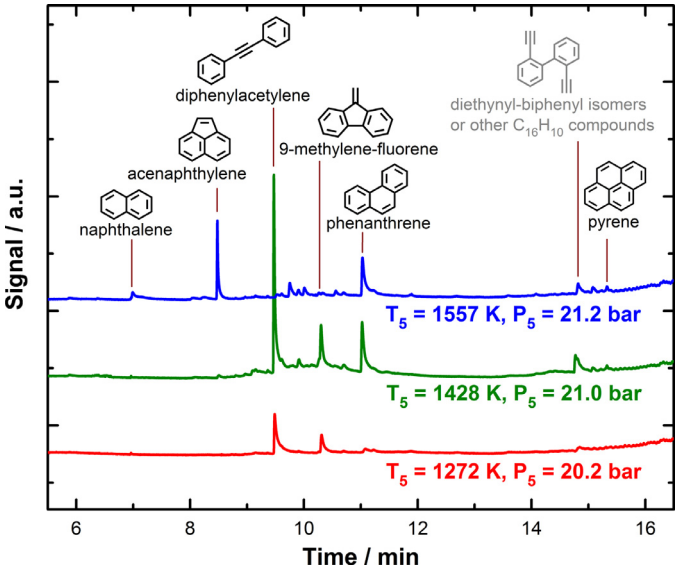

Fig. 1. GC signals (at the same scale) for PAH species produced from neat phenylacetylene ($C_6H_5C_2H$) pyrolysis at different post-shock temperatures (T_5s).

A 70 eV electron impact (EI) source is used for the ionization in the mass spectrometer which give mass spectra to match the fragmentation patterns in the NIST library. The detected unknown PAH peaks can have various isomers, some of which may have similar fragments, and in some cases the standard mass spectra are not available in the NIST library for all candidates. The mass spectrometry provides limited but crucial information, such as mass numbers for unknown species, even when they could not be unambiguously identified.

The GC signals for PAH compounds produced from neat phenylacetylene pyrolysis at different T_5 are shown in Fig. 1. The detected peaks are well separated and those of naphthalene ($C_{10}H_8$), acenaphthylene ($C_{12}H_8$), phenanthrene ($PC_{14}H_{10}$) and pyrene ($C_{16}H_{10}$) are identified according to their retention time. Diphenylacetylene ($C_6H_5CCC_6H_5$) and 9-methylene-fluorene ($C_{13}H_8CH_2$) are identified through their fragmentation patterns in the mass spectra. Their signals are already of considerable intensities at 1272 K, which further increase at 1428 K and diminish at the higher temperature of 1557 K. Phenanthrene and a species with the retention time of about 14.8 min also come into formation at 1272 K, and they both become more abundant at higher temperatures of 1428 K and 1557 K. The latter species, with the formula of $C_{16}H_{10}$ according to the mass number given by the mass spectrometry, can be fuel-related as it forms at the early stage of fuel consumption. It is assumed to be one of the diethynyl-biphenyl isomers, which are likely to be produced from the fuel radical ($C_6H_4C_2H$) self-recombination. Further experimental evidence will be required to confirm such a hypothesis. Naphthalene and acenaphthylene are only observed at a relatively high temperature of 1557 K, with acenaphthylene being of higher abundance. Pyrene already forms at 1428 K, but its level maintains low even at higher temperatures. Several small peaks, including the three between diphenylacetylene and 9-methylene-fluorene and the one appearing at around 10.5 min, all have the formula of $C_{14}H_8$. Their signal intensities increase with the temperature, and most of them only appear in the spectrum at 1557 K. Their high unsaturation degrees and high formation temperature windows indicate that they may come from the consumption of other PAH species, or through reactions involving acetylene at elevated temperatures. Potential candidates include diethynyl-naphthalene isomers and dehydrophenanthrene isomers, given the presence of naphthalene and phenanthrene and abundant ethynyl radicals at high temperatures.

The quantification of detected species relies on the calibration for the FID, as described in [26]. Except for diacetylene (C_4H_2), light species were calibrated with standard gas mixtures with known compositions supplied by Air Liquide. C_4H_2 was calibrated from C_2H_2 decomposition experiments through the carbon atom conservation. Gas-phase calibrations for two-ring PAH species, such as naphthalene, acenaphthylene, indene, biphenyl and bibenzyl, were performed with home-made mixtures. The process is similar to what was mentioned in a previous publication by Comandini et al. [28]. Solutions respectively containing different amounts of a specific PAH in methanol were prepared. Each solution was injected, in a small quantity (1–5 µl) using a syringe, into a 500 ml glass vessel which is equipped with a septum and heated up at 150 °C. The glass vessel was evacuated previously so that the solution vaporized immediately, and the vessel was subsequently filled with argon to a certain pressure. The gas mixture was allowed to stand for around 10–15 min before injection into the GC to guarantee good homogeneity. For larger PAH species which are difficult to directly calibrate, the gas-phase calibration factors were deduced from that of acenaphthylene by assuming that the relative signal intensities in liquid-phase remain in gas-phase. The liquid PAH calibration mixtures in acetonitrile were purchased from Sigma-Aldrich. The uncertainties in measured concentrations are within 10% for directly calibrated species, while for PAH species which were not calibrated in gas-phase, the uncertainties can vary from 20% to a factor of 2, depending on their relative molecular sizes to acenaphthylene. Qualitative and quantitative information, including retention time, peak concentrations and corresponding temperatures for PAH species measured in the current work is provided in Table 1.

In this work, three argon diluted mixtures respectively containing 103 ppm $C_6H_5C_2H$, 104 ppm $C_6H_5C_2H$+415 ppm C_2H_2 and 105 ppm $C_6H_5C_2H$+504 ppm C_2H_4, were used for the shock tube pyrolysis experiments at the nominal P_5 of 20 bar, covering a temperature range of 1100–1700 K. The different C_2H_x contents of the two binary fuel mixtures will not affect the validity of the experimental data for model development, though attention needs to be paid when directly comparing the experimental results among the three sets. For the used chemicals, phenylacetylene (98%) was purchased from Sigma-Aldrich, and the gas reagents including acetylene (>99.99%), ethylene (>99.99%) and argon (>99.9999%) were supplied by Air Liquide. Each mixture was prepared in a 136 L electropolished stainless steel cylinder and stayed overnight to homogenize before being used for the experiments. The driven section of the shock tube is heated at 90 °C to avoid the condensation of fuels and heavy products. The driven section is vacuumed to below 10^{-5} torr with a molecular turbo pump before each operation and the inner surface of the shock tube is cleaned every day to remove carbon deposits. The carbon balance for all identified products in the three experimental sets are provided in Fig. S1 in the Supplemental Material. In $C_6H_5C_2H_2/C_2H_2$ and $C_6H_5C_2H_4/C_2H_4$ pyrolysis, the carbon recoveries are over 96% at temperatures below 1450 K, while deteriorating at higher temperatures, to minima of 81% and 87%, respectively. This is mainly because larger polyacetylenes such as C_6H_2 and C_8H_2 are not identified in our experiments. In particular, relatively large amounts of C_6H_2 are expected to be produced at high temperatures from the decomposition of aromatic rings and the subsequent reactions among C_2H_2, C_2H, C_4H_2, and C_4H. A poorer carbon balance shows in the case of neat $C_6H_5C_2H$ pyrolysis, with a minimum recovery of 65% at 1557 K, indicating that larger amounts of heavy PAH species beyond detection might be formed in this case. But this hypothesis cannot be verified due to the incapability of measuring large polyacetylene compounds. The three data sets obtained in this work, including species con-

Table 1
A list of measured PAH species, along with their retention time, peak concentrations and corresponding temperatures and uncertainties in concentration measurements in neat phenylacetylene, phenylacetylene/acetylene and phenylacetylene/ethylene pyrolysis experiments.

Species	Formula	Retention time (min)	Neat phenylacetylene		Phenylacetylene/acetylene		Phenylacetylene/ethylene		Uncertainty in concentration measurements
			Peak concentration (ppm)	Peak temperature (K)	Peak concentration (ppm)	Peak temperature (K)	Peak concentration (ppm)	Peak temperature (K)	
naphthalene	$C_{10}H_8$	7.00	0.19	1533	0.54	1534	3.06	1548	10%
1-ethynyl- naphthalene	$C_{12}H_8$	8.24	0.19	1533	1.04	1514	0.77	1531	15%
acenaphthylene	$C_{12}H_8$	8.50	1.03	1576	4.70	1534	3.06	1586	10%
diphenylacetylene	$C_{14}H_{10}$	9.48	4.27	1468	2.09	1436	2.09	1424	20%
$C_{14}H_8$	$C_{14}H_8$	9.75	0.51	1533	1.31	1534	0.70	1586	30%
iso-	$C_{14}H_8$	9.96	0.20	1576	0.59	1557	0.36	1622	30%
mers[a]	$C_{14}H_8$	10.01	0.23	1557	0.81	1557	0.58	1622	30%
	$C_{14}H_8$	10.55	0.12	1515	0.48	1584	0.38	1622	30%
9-methylene-fluorene	$C_{14}H_{10}$	10.31	1.33	1428	1.16	1385	1.26	1375	20%
phenanthrene	$C_{14}H_{10}$	11.07	3.93	1515	4.69	1534	6.05	1519	20%
$C_{16}H_{10}$ isomers[b]	$C_{16}H_{10}$	14.82	1.10	1468	0.61	1522	1.03	1531	30%
pyrene	$C_{16}H_{10}$	15.32	0.17	1515	0.14	1585	0.24	1548	30%

[a] might be diethynyl-naphthalene and dehydrophenanthrene isomers.
[b] might by diethynyl-biphenyl isomers.

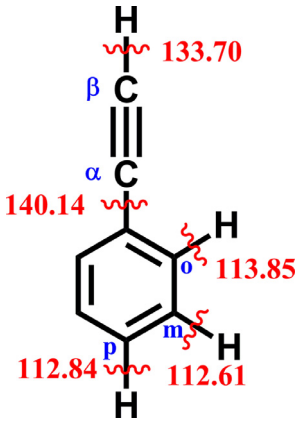

Scheme 2. The schematic of the phenylacetylene ($C_6H_5C_2H$) molecule and bond dissociation energies (BDEs) calculated at the ROCBS-QB3 [29] level of theory. (Unit: kcal/mol).

centrations, reaction time and end-wall pressure profiles for individual operations, are provided in the Supplemental Material.

3. Kinetic modeling

The current kinetic modeling efforts are aimed at depicting speciation from phenylacetylene decomposition as well as interpreting the interactions among the species pools, especially the pathways involved in PAH formation. The model development starts from the kinetic model for benzene and toluene pyrolysis proposed in our recent work [26], in which PAH formation kinetics starting from phenyl and benzyl radicals were refined on the basis of the latest version of CRECK model [3]. All updates made in the present work are listed in Table S1 in the Supplemental Material, with corresponding rate coefficients specified for each reaction. A glossary for nomenclature and structures of involved species is provided in Table S2. Important reactions will be discussed in detail in this section.

3.1. Phenylacetylene thermal decomposition

Although phenylacetylene ($C_6H_5C_2H$) is an important intermediate in the HACA route forming naphthalene, kinetic data on its decomposition are still scarce. The molecular structure of $C_6H_5C_2H$ and the bond dissociation energies (BDEs) calculated at the ROCBS-QB3 [29] level of theory are provided in Scheme 2. The indicated RO methodology eliminates the empirical corrections used in standard CBS-QB3 [30] to compensate for spin contamination [29]. The C–H bond strengths in the phenyl and ethynyl moieties are close to those in benzene (112.9 kcal/mol [31]) and acetylene (132.8 kcal/mol [31]), respectively.

The relatively high energies required to break the C–H bonds in $C_6H_5C_2H$ suggest its remarkable thermal stability, even compared to benzene. However, as shown in the Fig. 1, the emergence of pyrolysis products, indicating the decay of $C_6H_5C_2H$, occurs at relatively low temperatures (below 1300 K). Fission of a ring C–H bond (R1) is expected to be the main bond fission reaction initiating decomposition of $C_6H_5C_2H$. The corresponding o-, m- and p- radicals are lumped as $C_6H_4C_2H$ for the purpose of simplification in the current model. The only available rate coefficient for R1 is from shock tube experiments at a pressure of around 2 bar by Herzler and Frank [12]. We increased the original value by a factor of 5 to adjust to the current pressure of 20 bar. The adopted value $k_1 = 2.50 \times 10^{17}\exp(-56{,}870\ \mathrm{K}/T)\ \mathrm{cm^3\ mol^{-1}\ s^{-1}}$ is about 35–50% of the total rate constant for C–H bond fission in benzene reported by Sivaramakrishnan et al. [32] over the tempera-

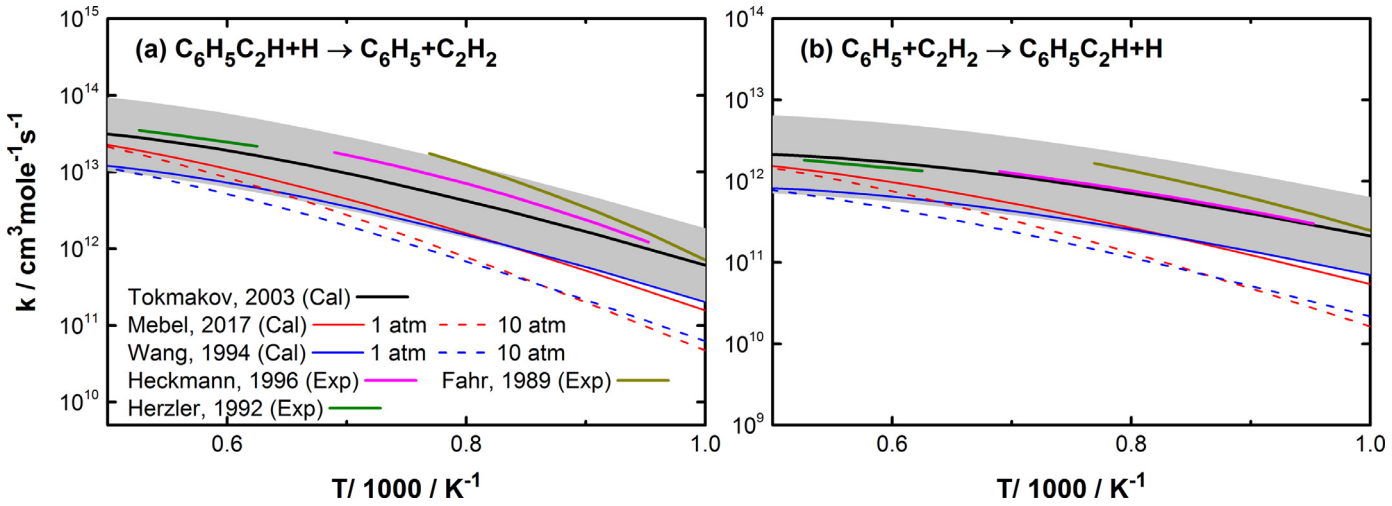

Fig. 2. Rate coefficients reported in literature for (a) R2, $C_6H_5C_2H+H$ => $C_6H_5+C_2H_2$ and (b) R-2, $C_6H_5+C_2H_2$ => $C_6H_5C_2H+H$. Measurements in [10,11] and calculations in [6,8,9] were for R-2 while the measurement in [12] was for R2. The reverse rate coefficients were computed through chemical equilibrium with the thermochemical data provided in [1]. The shadowed areas indicate three-fold uncertainties centered on the calculated rate coefficients for R-2 [8,33] and on the derived reverse rate coefficient for R2.

ture range of 1200–1700 K at nominal pressures of 30 and 50 bar. The mentioned rate expression in [32] was proposed to fit benzene decay profiles from their high-pressure shock tube pyrolysis experiments [32]. The current model also includes C–H bond fission in the ethynyl moiety, with the rate coefficient assigned as that for the C–H bond fission in acetylene.

$$C_6H_5C_2H = C_6H_4C_2H+H \quad (R1)$$

Bimolecular reactions between $C_6H_5C_2H$ and H atom occur in the reaction systems subsequent to the production of H atoms. Reactions of various types leading to different possible products (R2-R6) are extensively considered in the current model construction. In the early work by Herzler and Frank [12], only two channels were proposed, respectively producing $C_6H_5+C_2H_2$ (R2) and $C_6H_4C_2H+H_2$ (R3), and the rate coefficient was experimentally derived for R2, which was considered as the predominant pathway [12]. The reverse of R2, $C_6H_5+C_2H_2$ => $C_6H_5C_2H+H$ (R-2) is a crucial step of the HACA route leading to naphthalene formation from benzene; it also represents the prototypical addition of an aromatic radical to C_2H_2. Given its kinetic significance, R-2 has been investigated through both experimental [10,11] and theoretical [6,8,9] methods so that the corresponding rate coefficients k_{-2} are extensively available in literature. Rate coefficients for R2, k_2, including the direct measurement [12] and those derived from literature-reported k_{-2} [6,8–11] through chemical equilibrium, are compared in Fig. 2, in which k_{-2} with different origins are also shown. Theoretical works by Wang and Frenklach [6] and Mebel et al. [9] suggest a negative pressure-dependence of k_{-2}. However, weak pressure effects were shown in the calculated k_{-2} by Tokmakov and Lin [8], which agrees well with measurements over different temperature ranges [11,12] (see Fig. 2(b)). This rate constant [8,33] was used for the reversible reaction $C_6H_5+C_2H_2 = C_6H_5C_2H+H$ representing R2 in the current model. As shown in Fig. 2, for the chosen rate expression, three-fold uncertainties (between one third to three times of the nominal values) respectively centered on both forward and reverse rate coefficients can cover most available measurements and calculations at 1 atm in the temperature range of 1000–2000 K.

$$C_6H_5C_2H+H = C_6H_5+C_2H_2 \quad (R2)$$

$$C_6H_5C_2H+H = C_6H_4C_2H+H_2 \quad (R3)$$

$$C_6H_5C_2H+H = C_6H_6+C_2H \quad (R4)$$

$$C_6H_5C_2H+H = C_6H_5C\dot{H}C\dot{H} \quad (R5)$$

$$C_6H_5C_2H+H = C_6H_5\dot{C}CH_2 \quad (R6)$$

The rate coefficient $k_3 = 2.50 \times 10^4 \exp(-8052\ K/T)$ cm^3 mol^{-1} s^{-1} proposed in [1] was adopted for the hydrogen abstraction reaction (R3). With the current rate coefficients assignments, the hydrogen abstraction channel R3 takes a branching ratio of about 0.1 compared to R2 over the entire investigated temperature range, which is consistent with the value of <0.2 recommended in [12]. The reverse form of R4, $C_6H_6+C_2H = C_6H_5C_2H+H$, with a rate coefficient of $k_{-4} = 5.0 \times 10^{13}$ cm^3 mol^{-1} s^{-1}, was included in the kinetic model describing aromatics formation and growth by Wang and Frenklach [1]. This chemically-activated reaction was incorporated in the current model. Hydrogen addition reactions to the triple bond resulting in $C_6H_5C\dot{H}C\dot{H}$ and $C_6H_5\dot{C}CH_2$ radicals, R5 and R6, were also considered in the model construction, with the rate coefficients of the forward and reverse reactions separately specified with the values reported in [9] and [8]. The subsequent consumption of $C_6H_5C\dot{H}C\dot{H}$ and $C_6H_5\dot{C}CH_2$, including isomerization and decomposition steps, originated from the theoretical work by Tokmakov and Lin [8]. How these reactions compete resulting in $C_6H_5C_2H$ consumption will be revealed in the discussion section.

All the above-mentioned bimolecular reactions consume the chain carrier H atoms while producing radicals that are less reactive. However, phenylacetylene decomposes faster than benzene under similar shock tube pyrolysis conditions [26], which implies the existence of chain-branching processes enhancing the reactivity within the reaction system. In view of the abundant C_6H_5 resulting from R2, reactions between $C_6H_5C_2H$ and C_6H_5 were included in the model. Besides abstracting a hydrogen atom from $C_6H_5C_2H$, C_6H_5 can add to the triple carbon-to-carbon bond at the α or β site, producing two types of $C_{14}H_{11}$ adducts, $C_6H_5C(\dot{C}H)C_6H_5$ and $C_6H_5\dot{C}CHC_6H_5$, respectively (R7, R8). As shown in Scheme 3, $C_6H_5\dot{C}CHC_6H_5$ can decompose to diphenylacetylene ($C_6H_5CCC_6H_5$), meanwhile releasing an H atom (R9) via direct β-scission, or undergo intramolecular hydrogen transfer and cyclization steps leading to phenanthrene ($PC_{14}H_{10}$)+H (R10). The fate of $C_6H_5\dot{C}CHC_6H_5$ was theoretically explored by Matsugi and Miyoshi [2]. Apart from the dissociation channels, chemically activated reactions R11-R13 were

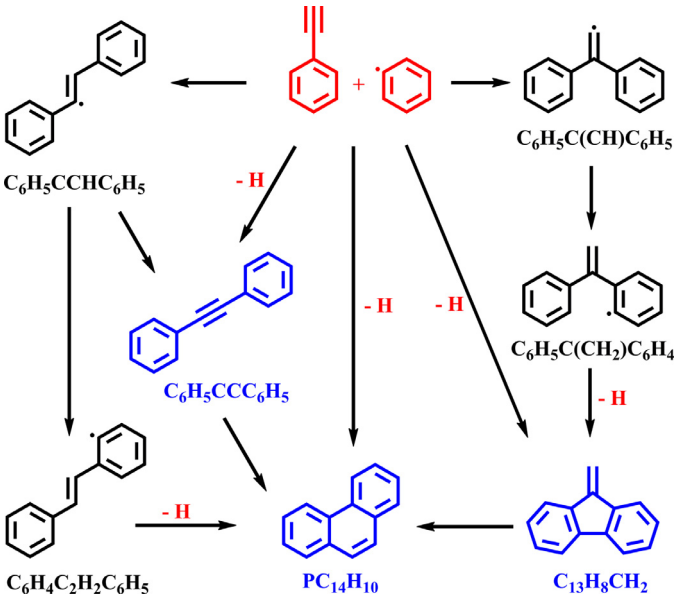

Scheme 3. Reaction sequences starting from C_6H_5 addition to the ethynyl branch of $C_6H_5C_2H$.

also identified on the same reaction potential energy surface (PES). If the original rate coefficients reported in [2] were used for R8-R13, obvious underestimation and over-prediction will show in the simulations for $C_6H_5CCC_6H_5$ and $PC_{14}H_{10}$ concentrations, respectively. Sensitivity analyses were performed for the two $C_{14}H_{10}$ isomers at T_5 = 1450 K where their concentrations are accumulating, and the results are provided in Fig. S2 in the Supplemental Material. A competition exists between the $C_6H_5CCC_6H_5$ and $PC_{14}H_{10}$ formation reactions shown in Scheme 3. Other important reactions that appear in the sensitivity spectra, such as $C_6H_5+C_2H_2 = C_6H_5C_2H+H$ (R2) and $C_6H_5+C_6H_5C_2H = C_6H_6+C_6H_4C_2H$, have similar, either facilitating or inhibiting, influences on both $C_6H_5CCC_6H_5$ and $PC_{14}H_{10}$, and these reactions also remarkably impact phenylacetylene decomposition reactivity. The currently investigated reaction system of phenylacetylene pyrolysis provides a good validation for the reaction pathways shown in Scheme 3, since both $C_6H_5CCC_6H_5$ and $PC_{14}H_{10}$ are important products starting to form at an early stage of phenylacetylene decomposition, and their concentration profiles were well quantified in the current experiments. Besides, uncertainties up to a factor of 3 are common in calculated rate coefficients for reactions involving species with such big sizes as C_{14}. Thus, to improve the model predictions for $C_6H_5CCC_6H_5$ and $PC_{14}H_{10}$ concentration measurements, adjustments within a factor of 3 were made for the rate coefficients of R10, R11 and R12.

$$C_6H_5C_2H+C_6H_5 = C_6H_5C(\dot{C}H)C_6H_5 \quad (R7)$$

$$C_6H_5C_2H+C_6H_5 = C_6H_5\dot{C}CHC_6H_5 \quad (R8)$$

$$C_6H_5\dot{C}CHC_6H_5 = C_6H_5CCC_6H_5+H \quad (R9)$$

$$C_6H_5\dot{C}CHC_6H_5 = PC_{14}H_{10}+H \quad (R10)$$

$$C_6H_5C_2H+C_6H_5 = C_6H_5CCC_6H_5+H \quad (R11)$$

$$C_6H_5C_2H+C_6H_5 = PC_{14}H_{10}+H \quad (R12)$$

$$C_6H_5CCC_6H_5+H = PC_{14}H_{10}+H \quad (R13)$$

The C_6H_5 addition occurring at the α site (R7) and the subsequent reactions were not investigated previously to the best of our knowledge. The resulting adduct $C_6H_5C(\dot{C}H)C_6H_5$ is likely to go through intramolecular hydrogen transfer and ring closure steps, leading to 9-methylene-fluorene ($C_{13}H_8CH_2$)+H, as presented in Scheme 3. Similar to the above-mentioned reaction sequences responsible for $PC_{14}H_{10}$ formation, stepwise conversion (R14–R15) and a chemically activated reaction (R16) were both considered for the formation of $C_{13}H_8CH_2$ in the current model. The rate coefficients for the C_6H_5 addition step (R7) and the chemically activated step (R16) were set equal to those of R8 and R12, respectively, by considering the kinetic similarities. The rate coefficient for the hydrogen transfer step (R14) was determined through an analogy to the isomerization between 2-phenyl-vinyl radical ($C_6H_5C\dot{C}H$) and 2-vinylphenyl radical ($C_6H_4C_2H_3$) [8]. The same rate coefficient was assigned to the ring closure step (R15) as for that of fluorene ($C_{13}H_{10}$) formation from o-benzyl-phenyl radical ($C_6H_5CH_2C_6H_4$) [34].

$$C_6H_5C(CH)C_6H_5 = C_6H_5C(CH_2)C_6H_4 \quad (R14)$$

$$C_6H_5C(CH_2)C_6H_4 = C_{13}H_8CH_2+H \quad (R15)$$

$$C_6H_5C_2H+C_6H_5 = C_{13}H_8CH_2+H \quad (R16)$$

The addition/elimination reaction of $C_6H_6+C_6H_5$ producing biphenyl ($C_6H_5C_6H_5$)+H as well as the reverse reaction were found to be of kinetic importance in benzene pyrolysis [26,35]. Such reactions may also take place between $C_6H_5C_2H$ and C_6H_5 or $C_6H_4C_2H$, leading to the formation of ethyl-biphenyl ($C_6H_4(C_2H)C_6H_5$) or diethynyl-biphenyl ($C_2HC_6H_4C_6H_4C_2H$) compounds, respectively (R17, R18). The rate constants for $C_6H_6+C_6H_5 = C_6H_5C_6H_5+H$ reported in [35] was adopted for both reactions with a three-fold increase, mainly to better capture phenylacetylene decomposition reactivity, according to sensitivity-analyzed results. The original rate constant from [35], covering a temperature range of 298–1330 K, was obtained through a combination of cavity ringdown spectrometry measurements at 40 Torr and theoretical calculations at the B3LYP/6–311G(d,p) level. Uncertainties of a factor of three could be common when it is used for analogous reactions under higher temperature and pressure conditions. Nevertheless, theoretical calculations are highly necessary to derive the rate coefficient for reactions which influence the reactivity of phenylacetylene in the future. The self-recombination of the $C_6H_4C_2H$ radical resulting in $C_2HC_6H_4C_6H_4C_2H$ (R19) was also considered, with the same rate coefficient of phenyl self-recombination [36] assigned. Both $C_6H_4(C_2H)C_6H_5$ and $C_2HC_6H_4C_6H_4C_2H$ are lumped species of isomers with different positions of ethynyl branches in the current model for simplification purpose.

$$C_6H_5C_2H+C_6H_5 = C_6H_4(C_2H)C_6H_5+H \quad (R17)$$

$$C_6H_5C_2H+C_6H_4C_2H = C_2HC_6H_4C_6H_4C_2H+H \quad (R18)$$

$$C_6H_4C_2H+C_6H_4C_2H = C_2HC_6H_4C_6H_4C_2H \quad (R19)$$

The $C_6H_5C_2H+C_6H_5$ and $C_6H_5C_2H+C_6H_4C_2H$ reactions discussed above can yield larger (C_{14} and C_{16}, accordingly) PAH species and meanwhile directly release H atoms. The inclusion of these reactions potentially accounts for the fast fuel consumption and the early formation of specific PAH species (see Fig. 1) as observed in the experiments.

3.2. Interactions between phenylacetylene and acetylene/ethylene

Another important goal of this work is to interpret the interactions between $C_6H_5C_2H$ and acetylene (C_2H_2) / ethylene (C_2H_4) under sooting combustion-relevant conditions where PAH formation pathways are prominent. Sub-mechanisms for C_2H_2 and C_2H_4

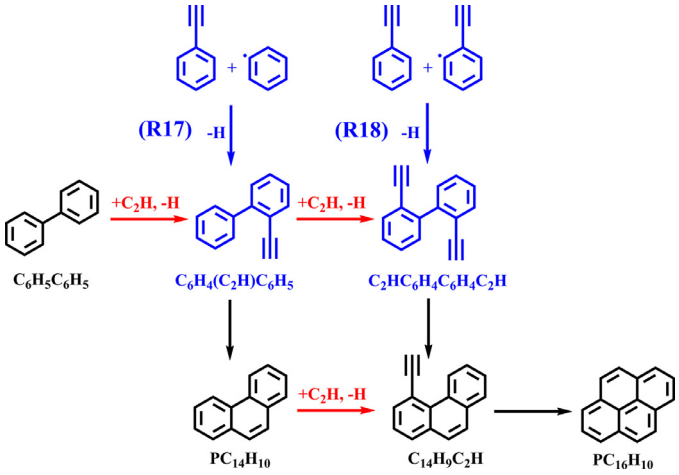

Scheme 4. Examples of the formation and conversion of PAH species containing ethynyl branches.

are already included in the C_0–C_4 core mechanism originating from the CRECK model [3], which however over-predict the decomposition rate of C_2H_4 in comparison to the current measurements. Our analysis found that the unimolecular decomposition to C_2H_2+H_2 was the predominant channel for C_2H_4 decay in the CRECK model [3]. In the current model, this reaction was removed and replaced with elementary steps from the well-validated USC Mech II [37], including C_2H_4 decomposing to H_2+vinylidene (H_2CC) (R20) and H_2CC isomerizing to C_2H_2 or participating in other reactions. The inclusion of the species H_2CC is rationalized by several theoretical studies [38,39] showing that the lowest-lying pathway for C_2H_4 decomposition is a 1,1-elimination of H_2 forming H_2CC which rapidly isomerizes to C_2H_2 over a small energy barrier of ~1 kcal/mol. Additionally, the rate coefficient of the hydrogen abstraction from C_2H_4 by H atom (R21) was updated with the value recommended by Baulch et al. [40].

$$C_2H_4(+M) = H_2 + H_2CC(+M) \quad \text{(R20)}$$

$$H + C_2H_4 = H_2 + C_2H_3 \quad \text{(R21)}$$

To check the reasonability of the modifications made in the C_2H_4 sub-mechanism, simulations were performed with or without the above-mentioned updates for the speciation in the heptane pyrolysis experiments reported in our previous work [26]. As the results presented in Fig. S3 in the Supplemental Material, model predictions for C_2H_4 concentrations are improved with the updated C_2H_4 reactions, especially at temperatures above 1500 K.

Reactions introduced by adding C_2H_2 or C_2H_4 to the reaction system of $C_6H_5C_2H$ decomposition, especially those contributing to PAH formation, are of particular interest in this study. Given the structure of $C_6H_5C_2H$, PAH species with ethynyl branches ($C_mH_nC_2H$) are expected to be abundant in the species pool. Adding C_2H_2 to the initial mixture will likely further enhance the formation of such species because of the contributions from two reaction types represented by R2 and R4, *i.e.* $C_mH_n+C_2H_2 = C_mH_nC_2H+H$ and $C_mH_{n+1} + C_2H = C_mH_nC_2H+H$, may intensify. Such reactions are explicitly considered in the current model with rate coefficients taken from the corresponding R2 and R4 reactions. As the examples in Scheme 4 illustrate, the products of the fuel-related reactions, R17 and R18, can also be formed by adding an ethynyl chain to the aromatic ring of relevant PAH species. The resulting $C_mH_nC_2H$ compounds with ethynyl branches at specific positions can give rise to ring growth through cyclization processes.

C_2H_4 and vinyl (C_2H_3), which contain double carbon-to-carbon bonds, are difficult to be produced directly from reactions of $C_6H_5C_2H$ under the current pyrolysis conditions. However, styrene ($C_6H_5C_2H_3$) is likely to be present in the species pool of the $C_6H_5C_2H$+C_2H_4 mixture pyrolysis, for instance, produced through the chemically activated reaction C_6H_5+C_2H_4 = $C_6H_5C_2H_3$+H [41]. Reactions responsible for the consumption of $C_6H_5C_2H_3$ were updated based on the kinetic model for $C_6H_5C_2H_3$ combustion proposed by Yuan et al. [14]. Styrene radicals, 1-styryl ($C_6H_5\dot{C}HCH$) and o-vinylphenyl ($C_6H_4C_2H_3$) are sufficiently stable at high pressures to facilitate the Bittner-Howard route [42] and the modified Frenklach route [43], which both contribute to $C_{10}H_8$ formation [9]. In the modified Frenklach route, the adduct $C_6H_4(CHCH_2)(C\dot{H}CH)$ produced from the C_2H_2 addition to $C_6H_4C_2H_3$ goes through six-member ring-closure giving $C_{10}H_8$+H [9]. In the currently concerned $C_6H_5C_2H$+C_2H_4 reaction system, $C_6H_5C_2H$+C_2H_3 and $C_6H_4C_2H$+C_2H_4 are both potential sources of $C_6H_4(CHCH_2)(C\dot{H}CH)$ which predominantly converts to $C_{10}H_8$. The above-mentioned reactions, representing kinetic interplays between $C_6H_5C_2H$ and C_2H_x, potentially alter the fuel consumption schemes and the production of PAH species in the pyrolysis of binary fuel mixtures. Their roles in the reaction systems will be illustrated by experimental evidence and modeling analyses in the following discussion section.

221 species and 3542 reactions are included in the current kinetic model. The reaction mechanism and thermochemical data are provided in the Supplemental Material. Thermochemical data for most species come from the CRECK model [3] since it is the basis of the current model. For species introduced by reactions added or updated in this work, their thermochemical data originate from the same publications [6,34] as corresponding reactions. For some reactions, theoretically computed rate constants from both forward and reverse directions are available, so they are expressed in a pair of irreversible reactions with separate rate constants in the model. This practice can help to eliminate the errors in reaction rates brought by the uncertainties and potential inconsistency in the thermochemical data. All simulations in the current work were performed with the homogenous reactor model of the software COSILAB [44]. The nominal reaction time of 4.0 ms and the constant pressure of 20 bar were used in the simulations. The constant pressure assumption typically used in simulating the speciation results sampled from single-pulse shock tube experiments has been well justified in previous publications [45,46]. It was suggested [47,48] that in specific cases, important fractions of some products might be formed through reactions involving stable radicals in the post-shock cooling period, so that the modeling results would be distorted. Simulations with measured pressure profiles were performed over a longer time scale (8.0 ms) around T_5 = 1450 K in the respective cases of neat $C_6H_5C_2H$, $C_6H_5C_2H$+C_2H_2 and $C_6H_5C_2H$+C_2H_4 pyrolysis. The time dependent concentrations of major products and important radicals are shown in Fig. S4 in the Supplemental Material. The currently investigated reaction systems do not produce large amounts of highly-stabilized radicals such as benzyl, which can be present in large amounts when the reaction quenching starts. In addition, concentrations of the major radicals including H, C_6H_5 and $C_6H_4C_2H$ are too low to substantially impact the final product amounts. The plateaus in the concentrations of the major products during quenching processes indicate that their formation is already completed by this time.

4. Discussion

In this section, the first step is to shed light on the fuel decomposition reactivity and speciation behaviors of $C_6H_5C_2H$ pyrolysis through joined experimental observations and modeling inter-

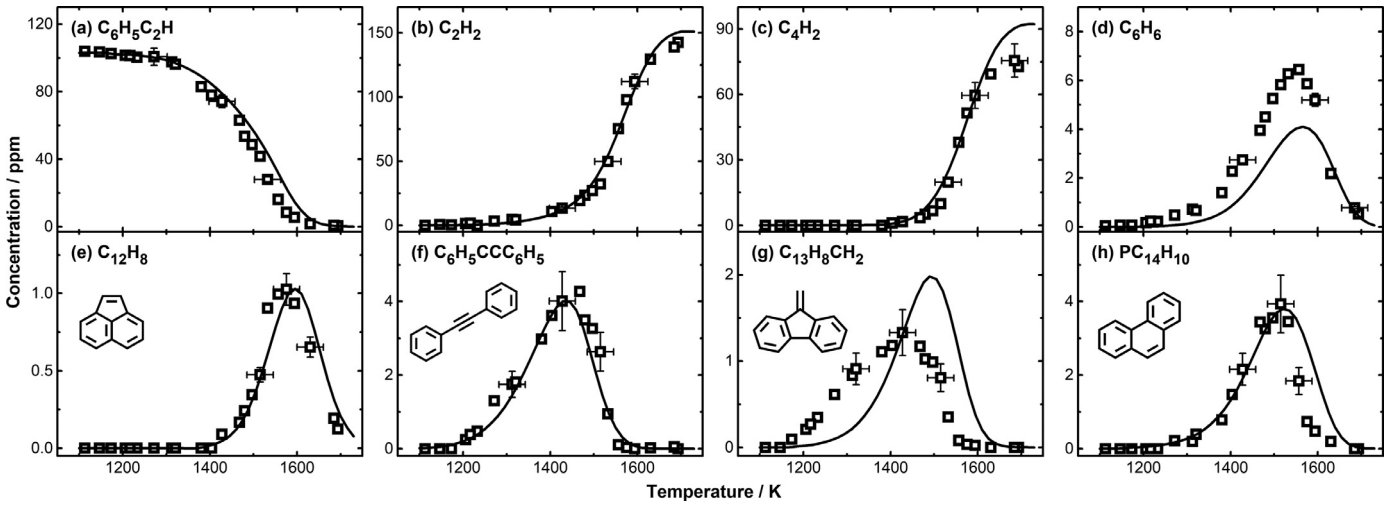

Fig. 3. Measured (symbols) and simulated (lines) concentration profiles for fuel and major products with peak concentrations over 1 ppm in 103 ppm phenylacetylene pyrolysis experiments.

pretations. The kinetic model is validated with the measurements as the prerequisite for relevant modeling analyses. The subsequent step is to reveal the influences of added C_2H_2 and C_2H_4 on the speciation patterns of $C_6H_5C_2H$ pyrolysis, with particular attention paid to the PAH formation pathways. To this end, the species pools and reaction schemes of $C_6H_5C_2H$+C_2H_2 and $C_6H_5C_2H$+C_2H_4 pyrolysis are compared with those of neat $C_6H_5C_2H$ pyrolysis.

4.1. Fuel decomposition and species formation during phenylacetylene pyrolysis

Measured and simulated for the fuel, the major products C_2H_2 and C_4H_2 and selected intermediates in neat phenylacetylene pyrolysis are shown as a function of the temperature in Fig. 3. The current model satisfactorily captures the fuel reactivity and speciation profiles with respect to both the temperature windows and the peak concentrations. To gain insights into the detailed chemistry within the reaction system, rate-of-production (ROP) analyses were performed at 1450 K, where about half of the fuel is consumed and the shown PAH compounds have considerable concentrations. A reaction network depicting how $C_6H_5C_2H$ consumption results in species formation is established based on the ROP-analyzed results and displayed in Fig. 4.

As can be noted, the chemically-activated reaction $C_6H_5C_2H$+H = C_6H_5+C_2H_2 (R2) dominates the fuel consumption at 1450 K. It also plays an important role at lower temperatures where $C_6H_5C_2H$ decomposition has just begun. This is suggested by the early formation of C_2H_2 (See Fig. 2(b)), a phenomenon not seen in the pyrolysis of benzene and toluene under similar conditions [26]. In R2, a chain carrier H atom is consumed, producing a C_6H_5, which is both less reactive than H and may consume additional H through C_6H_5 + H recombination. One might think that the loss of the chain carrier H atoms would reduce reactivity; to reveal the mechanism that maintains reactivity, sensitivity analyses of the fuel concentration were performed at1350 K, 1450 K and 1550 K, and the results are shown in Fig. S5. At all examined temperatures, R2 is seen to dominate $C_6H_5C_2H$ conversion, a result we attribute to the subsequent attack of C_6H_5 on $C_6H_5C_2H$, leading to the release of H atoms through both stepwise and direct pathways, as highlighted in Fig. 4. These processes also generate the observed $C_{14}H_{10}$ compounds. Formation of $C_6H_5CCC_6H_5$ is the largest product channel from $C_6H_5C_2H$+C_6H_5. At higher temperatures $C_6H_5CCC_6H_5$ becomes an intermediate and the carbon reservoir shifts to $PC_{14}H_{10}$ through H assisted isomerization ($C_6H_5CCC_6H_5$+H = $PC_{14}H_{10}$+H, R13). This accounts for the different formation temperature windows of $C_6H_5CCC_6H_5$ and $PC_{14}H_{10}$ observed in the experiments (see Fig. 4). The current model can well capture the speciation profiles of $C_6H_5CCC_6H_5$ and $PC_{14}H_{10}$, regarding both the shape and the size. Improvements are still required to more correctly characterize the formation temperature window for another $C_{14}H_{10}$ product $C_{13}H_8CH_2$. The currently used rate coefficients of relevant reactions (R7, R14-R16) were evaluated based on analogies to similar reactions. Future theoretical efforts towards more accurate kinetic parameters for the reaction system of $C_6H_5C_2H$+C_6H_5 are definitely desired. Other radical+molecule addition/elimination reactions releasing H atoms also have minor contributions to the system reactivity, as can be identified in Fig. 4: $C_6H_5C_2H$ reacts also with its radical $C_6H_4C_2H$, similar to the case of $C_6H_5C_2H$+C_6H_5, simultaneously producing a $C_{16}H_{10}$ PAH species ($PC_{16}H_{10}$ or $CH_2C_6H_4C_6H_4CH_2$) and an H atom. Ethynyl (C_2H) radicals can also generate free H atoms by adding to aromatic rings and displacing the H atoms. Due to the importance of R2 in sustaining the system reactivity, the competing channels (R3, R4) have negative effects on the consumption of $C_6H_5C_2H$ (see Fig. S5), even though they can contribute to the formation of $C_6H_4C_2H$ and C_2H, both of which can also displace H atoms from aromatic rings, similar to C_6H_5. The difference lies in alternative consumption channels of the three radicals besides the addition-elimination reactions regenerating H atoms. C_6H_5 also undergoes fragmentation eventually leading to C_2H_2+C_4H_2+H. This pathway, having increasing contributions with the temperature, also results in the generation of H atoms. However, for $C_6H_4C_2H$ and C_2H, other important consumption pathways, *i.e.* $C_6H_4C_2H$+C_2H_2 → $C_9H_6CH/C_{10}H_7$ and C_2H+$C_6H_5C_2H$ → $C_6H_4C_2H$+C_2H_2, respectively, cannot produce reactive chain carriers. The fate of $C_6H_4C_2H$ relevant to PAH formation constitutes a key consideration of this work. The C_2H_2 addition to $C_6H_4C_2H$ is an essential step in the HACA route leading to formation of naphthyl radical. The C_2H_2 addition reactions are very important in $C_6H_4C_2H$ consumption, only second to the above-mentioned reaction $C_6H_5C_2H$+$C_6H_4C_2H$ = $CH_2C_6H_4C_6H_4C_2H$+H, at the analyzed temperature of 1450 K, and their importance further increases at higher temperatures. The detailed reaction mechanism of $C_6H_4C_2H$+C_2H_2 was investigated by Mebel et al. [9], and the reported rate coefficients were incorporated into the current model. The channels leading to benzofulvenyl (C_9H_6CH) and naphthyl ($C_{10}H_7$) are dominant and of comparable branching ratios under the currently investigated temperature and pressure

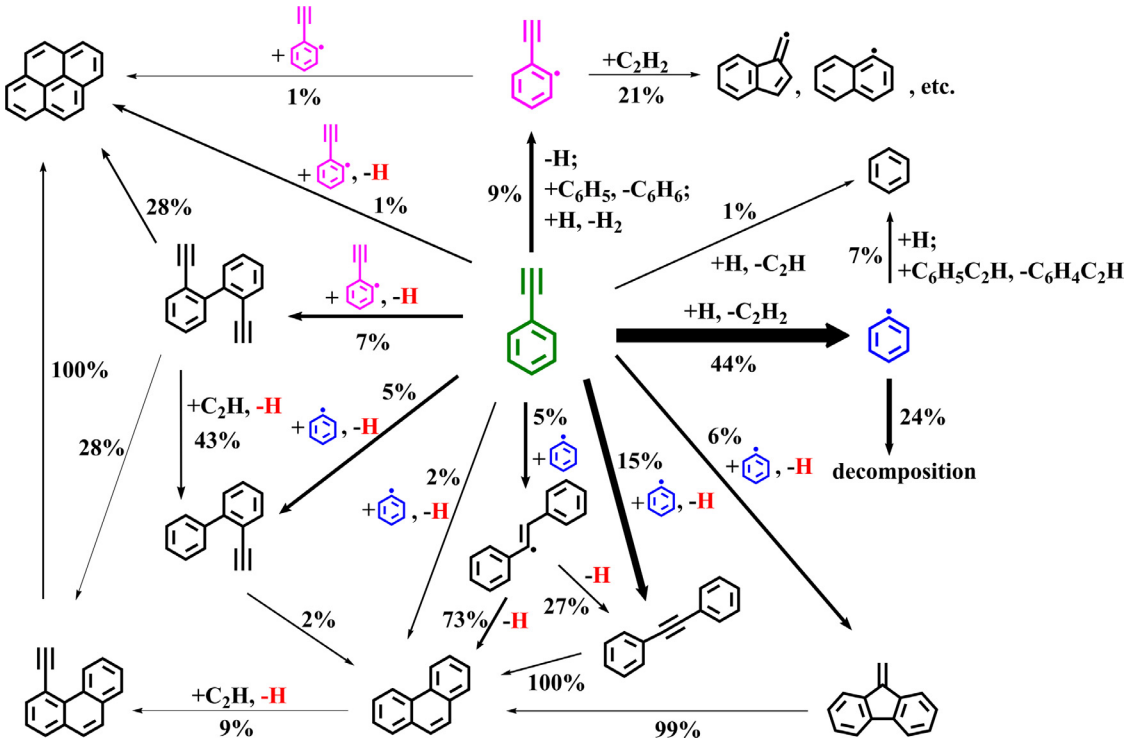

Fig. 4. Reaction pathways of species formation from fuel consumption at P_5 = 20 bar and T_5 = 1450 K in neat phenylacetylene pyrolysis. The thickness of the arrows represents the carbon flux through the corresponding reaction. The numbers are the percentage contributions of corresponding reactions to the consumption of species on the source side of the arrows.

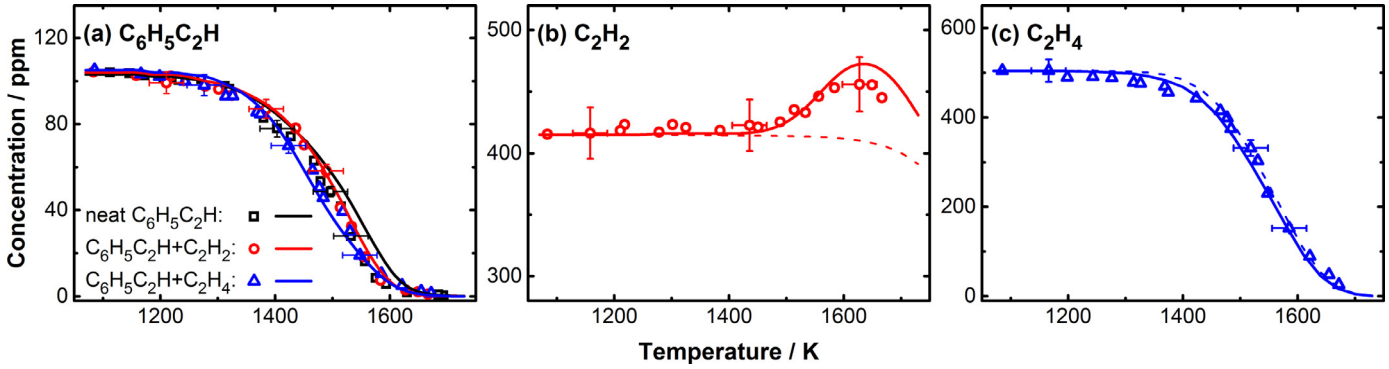

Fig. 5. Experimental (symbols) and simulated (solid lines) concentrations of (a) $C_6H_5C_2H$ in the three investigated cases, (b) C_2H_2 in the pyrolysis of 104 ppm $C_6H_5C_2H$ + 415 ppm C_2H_2 mixture and (c) C_2H_4 in the pyrolysis of 105 ppm $C_6H_5C_2H$ + 504 ppm C_2H_4 mixture. The dashed lines in (b) and (c) represent the simulated concentrations of C_2H_2 and C_2H_4 when $C_6H_5C_2H$ is absent from corresponding mixtures.

condition. Both radicals continue reacting with C_2H_2, ending up in $C_{12}H_8$, while "skipping" the formation of $C_{10}H_8$ which requires the participation of an H atom. This accounts for the negligible concentration of $C_{10}H_8$ produced in $C_6H_5C_2H$ pyrolysis. The HACA pathways have more pronounced contributions at elevated temperatures where C_2H_2 is of considerable abundance. This explains the higher peak temperature of $C_{12}H_8$ concentration (see Fig. 2(e)), compared to those of the three $C_{14}H_{10}$ isomers produced from fuel-related pathways.

4.2. Influences of added acetylene and ethylene on phenylacetylene consumption and small intermediates formation

First, the influences of the abundant C_2H_2 or C_2H_4 on $C_6H_5C_2H$ decomposition reactivity is inspected. Concentration profiles of $C_6H_5C_2H$ in all three experimental sets, and those of C_2H_2 and C_2H_4 when they have been added as initial components are shown in Fig. 5. The current model can well capture the decomposition reactivity of $C_6H_5C_2H$ in three separate cases throughout the investigated temperature range with the experimental uncertainties taken into consideration. Due to an uncertainty of ±30 K in the experimentally determined T_5, the small differences in the $C_6H_5C_2H$ decomposition rates for the three mixtures are not definitive. However, the modeling results indicate that C_2H_2 slightly promotes the consumption of $C_6H_5C_2H$ above 1500 K, and that C_2H_4 has a larger accelerating effect on $C_6H_5C_2H$ decay. C_2H_2 and C_2H_4 concentrations evolve very differently with temperature in the respective cases, because C_2H_2 is a major product from $C_6H_5C_2H$ pyrolysis which barely contributes to C_2H_4 formation. Model-predicted C_2H_2 and C_2H_4 concentration profiles when $C_6H_5C_2H$ is replaced by argon in corresponding mixtures are also shown in Fig. 5 to illustrate the distinct decomposition reactivity of C_2H_2 and C_2H_4. The slight consumption of C_2H_2 is compensated by its production from $C_6H_5C_2H$ decomposition. C_2H_4 decomposes more slowly than $C_6H_5C_2H$. The slight increase in the decomposition rates of $C_6H_5C_2H$ and C_2H_4 when both are present indicates a "synergis-

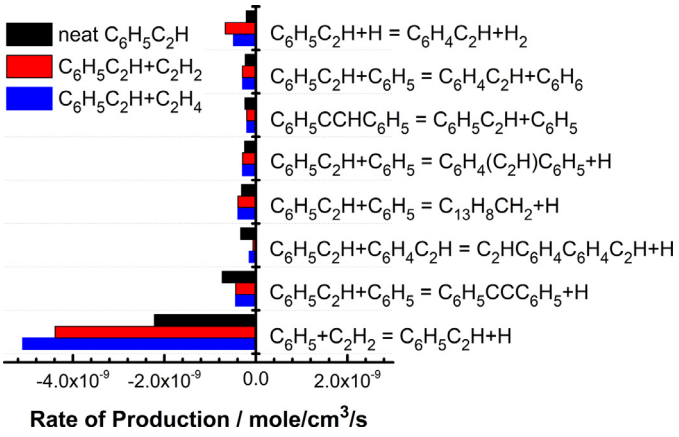

Fig. 6. ROP-analyzed results for $C_6H_5C_2H$ consumption at T_5 = 1450 K and P_5 = 20 bar in the pyrolysis of neat $C_6H_5C_2H$, $C_6H_5C_2H+C_2H_2$ and $C_6H_5C_2H+C_2H_4$ mixtures.

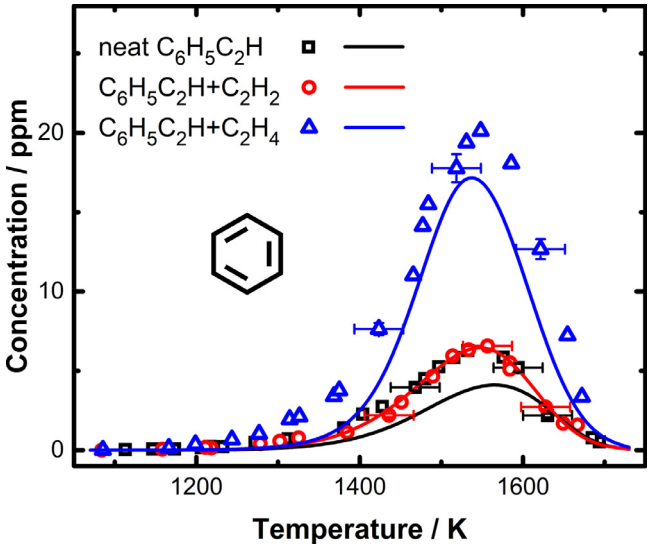

Fig. 7. Experimental (symbols) and simulated (lines) concentrations of C_6H_6 in the pyrolysis of 103 ppm $C_6H_5C_2H$, 104 ppm $C_6H_5C_2H$ + 415 ppm C_2H_2 and 105 ppm $C_6H_5C_2H$ + 504 ppm C_2H_4.

tic effect" in the pyrolysis of $C_6H_5C_2H+C_2H_4$ mixture, which is caused by crosslink reactions: the decomposition of C_2H_4 produces H atoms, thus accelerating the decomposition of phenylacetylene through $C_6H_5C_2H+H = C_6H_5+C_2H_2$ (R2); the resulting C_6H_5 can promote the consumption of C_2H_4 via the reaction $C_6H_5+C_2H_4 = C_6H_5C_2H_3+H$, and release an H atom at the same time.

Rate-of-Production (ROP) analysis for phenylacetylene consumption was performed at T_5 = 1450 K and P_5 =20 bar to reveal the chemical details responsible for the different model-predicted $C_6H_5C_2H$ decomposition reactivity among the three cases, and the results are shown in Fig. 6. R2 plays a dominant role in all three cases and it results in more $C_6H_5C_2H$ consumption in the pyrolysis of the binary fuel mixtures containing either C_2H_2 or C_2H_4, as a consequence of the increased level of H atoms, especially in $C_6H_5C_2H+C_2H_4$ pyrolysis. Compared to neat $C_6H_5C_2H$ pyrolysis, the hydrogen abstraction by H atom (R3) contributes more in $C_6H_5C_2H+C_2H_2$ and $C_6H_5C_2H+C_2H_4$ pyrolysis. Contrarily, the reactions of $C_6H_5C_2H+C_6H_5$ and $C_6H_5C_2H+C_6H_4C_2H$, which assist the production of H atoms, are less important if C_2H_2 or C_2H_4 is added. The decomposition of C_2H_4 is a more efficient source of H atoms compared with $C_6H_5C_2H$ or C_2H_2. This can partly explain the enhanced formation of C_6H_6 through C_6H_5+H recombination in the $C_6H_5C_2H+C_2H_4$ mixture. As shown in Fig. 7, the peak concentration of C_6H_6 in $C_6H_5C_2H+C_2H_4$ pyrolysis is much higher than those in the other two cases. ROP analysis was performed to reveal the different formation schemes of C_6H_6 in the three cases at T_5 = 1550 K, where the C_6H_6 concentrations are approaching their peaks. The results, as a function of the reaction time, are shown in Fig. 8.

Three reactions play important roles in all cases, including the hydrogen abstraction from $C_6H_5C_2H$ by C_6H_5 ($C_6H_5C_2H+C_6H_5 = C_6H_4C_2H+C_6H_6$), the recombination of C_6H_5+H and the bimolecular reaction between $C_6H_5C_2H$ and H leading to $C_6H_6+C_2H$ (R4). The higher C_6H_6 production through the two latter reactions in $C_6H_5C_2H+C_2H_x$ pyrolysis than that in neat $C_6H_5C_2H$ pyrolysis is thanks to the more abundant H atoms, as mentioned above. Besides, the added C_2H_x can both donate an H atom to C_6H_5 to result in C_6H_6 formation, through $C_2H_2+C_6H_5 = C_2H+C_6H_6$ and $C_2H_4+C_6H_5 = C_2H_3+C_6H_6$ in the pyrolysis of $C_6H_5C_2H+C_2H_2$ and $C_6H_5C_2H+C_2H_4$ pyrolysis, respectively. This channel has a more notable contribution in $C_6H_5C_2H+C_2H_4$ pyrolysis as hydrogen abstraction from C_2H_4 is remarkably easier. Moreover, in $C_6H_5C_2H+C_2H_4$ pyrolysis, the consumption reactions of styrene ($C_6H_5C_2H_3$), $C_6H_5C_2H_3 = C_6H_6+H_2CC$ and $C_6H_5C_2H_3+H = C_6H_6+C_2H_3$ have important contributions, and particularly, the former reaction is the predominant C_6H_6 formation pathway. As can be seen in Fig. 8, the effects of the two $C_6H_5C_2H_3$ reactions are delayed in comparison to other C_6H_6 formation channels, owing to the concentration build-up of $C_6H_5C_2H_3$ as an intermediate in $C_6H_5C_2H+C_2H_4$ pyrolysis. $C_6H_5C_2H_3$ is absent from the species pools of neat $C_6H_5C_2H$ and $C_6H_5C_2H+C_2H_2$ pyrolysis, and it is a representative product resulting from the interactions between $C_6H_5C_2H$ and C_2H_4 consumption. Its concentration profiles as a function of the temperature is presented in Fig. 9 together with those of other small molecule products in the pyrolysis of $C_6H_5C_2H$ + C_2H_2 and $C_6H_5C_2H$ + C_2H_4. As mentioned above, C_2H_4 cannot be produced from the pyrolysis of neat $C_6H_5C_2H$ or $C_6H_5C_2H+C_2H_2$ mixture, since these environments are highly unsaturated. C_2H_4 in the initial gas mixtures thus introduces new species to the intermediates pool. Light species such as methane (CH_4), allene (a-C_3H_4) and propyne (p-C_3H_4), which were under the detection limit in the other two experimental sets, were observed in the pyrolysis of $C_6H_5C_2H$ + C_2H_4. As mentioned in the kinetic modeling section, C_2H_4 consumption reactions were modified in the current model to capture C_2H_4 decomposition reactivity. Simulated concentration profiles of small products in $C_6H_5C_2H+C_2H_4$ pyrolysis, with a model excluding the modifications, are shown as the thin dash-dotted lines in Fig. 9. No modifications were made in the kinetic model specifically to match the measurements of small intermediates. But with the updates in C_2H_4 reactions, the agreement between the measurements and the simulations for C_1–C_4 hydrocarbon concentration profiles is significantly improved, though CH_4 concentrations are still under-predicted at high temperatures. This further justifies the modifications made to improve the prediction for C_2H_4 reactivity in the current model.

4.3. Impacts of added acetylene and ethylene on PAH formation

To reveal the interactions between $C_6H_5C_2H$ and C_2H_2 or C_2H_4, which alter the formation patterns of PAH species, is a crucial target in this study. Figure S6 exhibits the GC signals for PAH species in the three reaction systems at two different temperatures around 1380 K and 1530 K. The former represents the initial stage of $C_6H_5C_2H$ decomposition, at which the $C_6H_5C_2H$-related

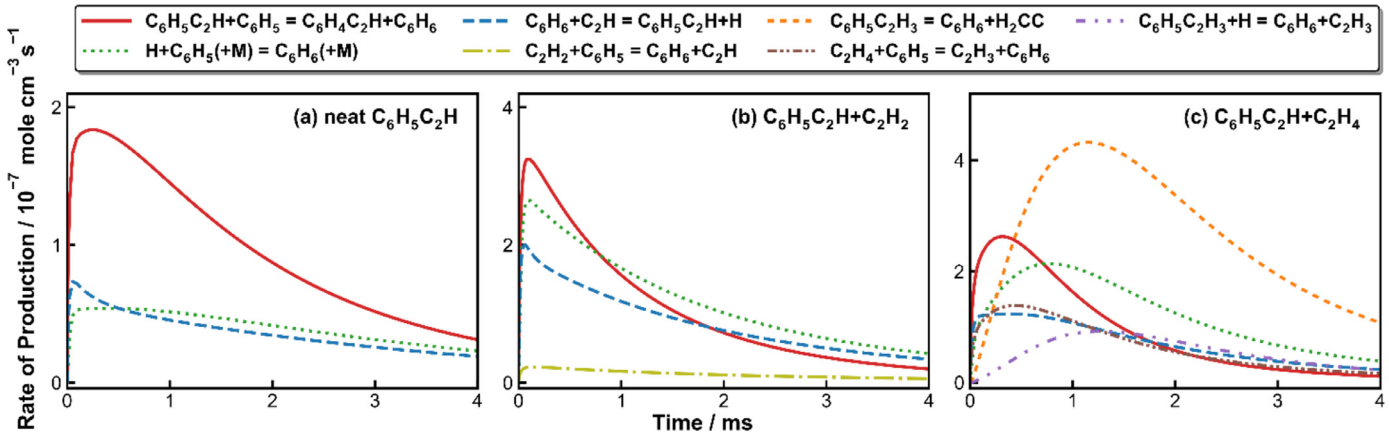

Fig. 8. ROP analysis for C_6H_6 production over the reaction time in the pyrolysis of (a) neat $C_6H_5C_2H$, (b) $C_6H_5C_2H$+C_2H_2 and (c) $C_6H_5C_2H$+C_2H_4 at T_5 = 1550 K and P_5 = 20 bar.

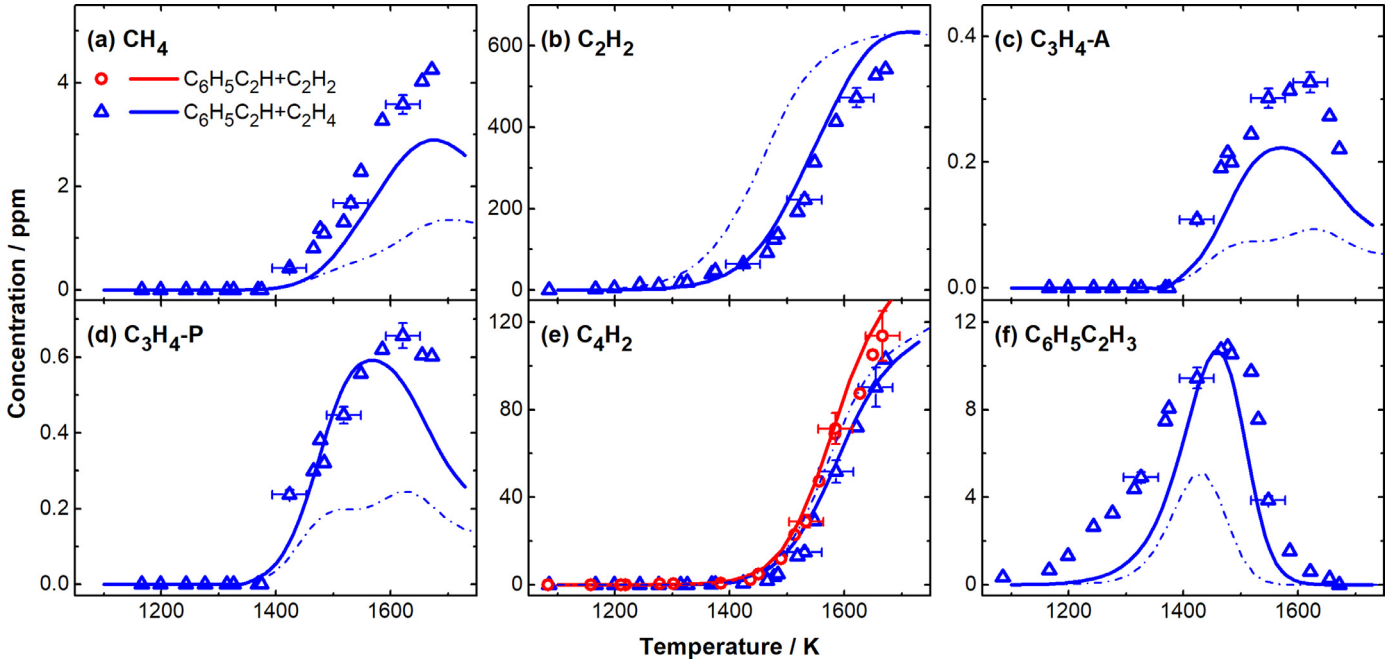

Fig. 9. Measured (symbols) and simulated (lines) concentrations of small molecule products as a function of T_5 from the pyrolysis of 104 ppm $C_6H_5C_2H$ + 415 ppm C_2H_2 and 105 ppm $C_6H_5C_2H$ + 504 ppm C_2H_4 mixtures at the nominal P_5 of 20 bar. The thin dash-dotted lines are simulations in $C_6H_5C_2H$+C_2H_4 pyrolysis with a kinetic model without the modifications of C_2H_4 reactions made in this work.

pathways prevail. While the latter is typical in the high temperature regime where $C_6H_5C_2H$ is depleting and the general pathways, such as the HACA routes, may play a more significant role. It is noteworthy that at 1380 K the production of $C_6H_5CCC_6H_5$ is inhibited when either C_2H_2 or C_2H_4 is present in the initial testing gas mixture, and the early formation of $C_{12}H_8$ and $C_{10}H_8$ occurs in the cases of $C_6H_5C_2H$+C_2H_2 and $C_6H_5C_2H$+C_2H_4, respectively. At 1530 K, compared to the species pool of neat $C_6H_5C_2H$ pyrolysis, the extra C_2H_2 results in an obvious peak of 1-ethynylnaphthalene ($C_{10}H_7C_2H$) and significant increases in the intensities of $C_{12}H_8$ and the small peaks of the $C_{14}H_8$ compounds. The introduction of C_2H_4 to the reaction system promotes the formation of the two- to four- ring primary PAHs, *i.e.* naphthalene ($C_{10}H_8$), phenanthrene ($PC_{14}H_{10}$) and pyrene ($PC_{16}H_{10}$).

Experimental and simulated concentrations of the PAH species, including the ambiguously identified $C_2HC_6H_4C_6H_4C_2H$ and the $C_{14}H_8$ isomers, as a function of the temperature are shown in Fig. 10, for a comparison of the PAH speciation behaviors among the three investigated cases. Overall, the current kinetic model can satisfactorily reproduce the shown concentration profiles within the experimental uncertainties, and more importantly, the model captures the variation in the PAH species trends with respect to peak concentrations and the corresponding temperatures when changing the initial fuel compositions. The three experimental data sets show no obvious differences in the temperatures of peak formation of the three $C_{14}H_{10}$ isomers, as shown in the second row of Fig. 10. However, in the binary mixtures, the peak concentration of $C_6H_5CCC_6H_5$ is half of that seen in neat $C_6H_5C_2H$ pyrolysis, as a result of the reduced contribution of $C_6H_5C_2H$+C_6H_5 = $C_6H_5CCC_6H_5$+H when unsaturated C_2 species are present (see Fig. 6). $C_{10}H_8$ starts to be produced at a relatively low temperature and the peak concentration is much higher in the case of $C_6H_5C_2H$+C_2H_4 pyrolysis. The early formation and enhanced peak concentrations of acenaphthylene ($C_{12}H_8$) and its non-ring-fused isomer 1-ethynylnaphthalene ($C_{10}H_7C_2H$) are seen in the pyrolysis of $C_6H_5C_2H$+C_2H_2. The addition of C_2H_4 to the fuel

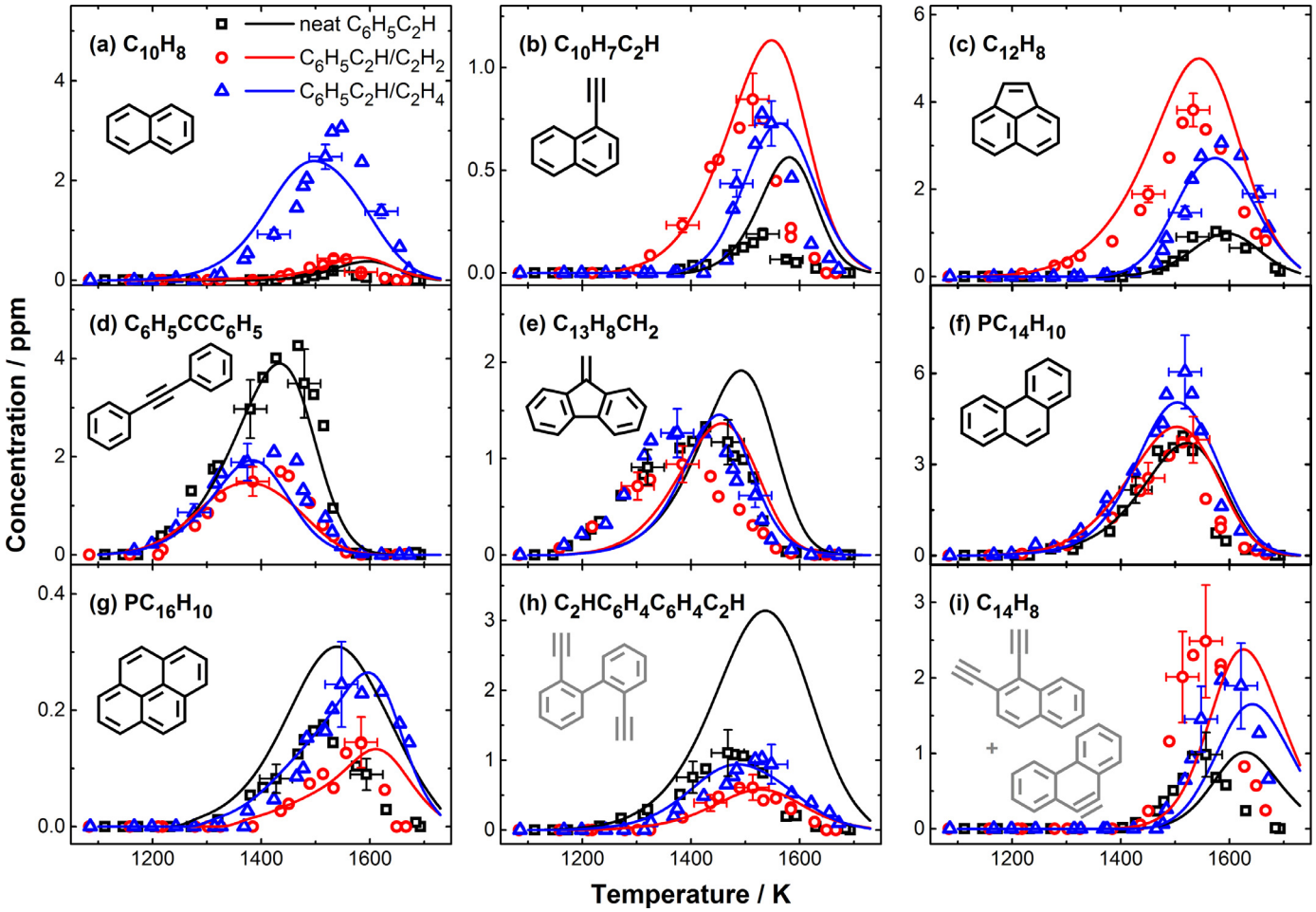

Fig. 10. Experimental (symbols) and simulated (lines) concentrations of PAH species as a function of T_5 in the pyrolysis of 103 ppm $C_6H_5C_2H$, 104 ppm $C_6H_5C_2H$ + 415 ppm C_2H_2 and 105 ppm $C_6H_5C_2H$ + 504 ppm.

mixture amplifies the concentrations of $C_{12}H_8$ and $C_{10}H_7C_2H$ in the same temperature window, but to a lesser degree.

To obtain detailed kinetic insights into the remarkable influences on naphthalene ($C_{10}H_8$) and acenaphthylene ($C_{12}H_8$) production brought by added C_2H_2 and C_2H_4, sensitivity analyses were performed for $C_{10}H_8$ and $C_{12}H_8$ at T_5 = 1500 K, where concentrations of both PAH species increase at significantly different rates among the three experimental sets. Figure 11 presents the results in the pyrolysis of neat $C_6H_5C_2H$, $C_6H_5C_2H$+C_2H_2 and $C_6H_5C_2H$+C_2H_4. It is noted that $C_{10}H_7$+H(+M) = $C_{10}H_8$(+M) and C_2H_2+$C_6H_4C_2H$ => $C_{10}H_7$ are the most sensitive reactions promoting $C_{10}H_8$ formation in both neat $C_6H_5C_2H$ pyrolysis and $C_6H_5C_2H$+C_2H_2 pyrolysis, in which $C_{10}H_8$ formation relies on the conversion of $C_{10}H_7$ produced through the HACA route. However, the limited H atoms produced in these two highly unsaturated reaction systems, are mainly consumed by reacting with $C_6H_5C_2H$ and the conversion of $C_{10}H_7$ to $C_{10}H_8$ is far less competitive. In $C_6H_5C_2H$+C_2H_4 pyrolysis, the above-mentioned reactions are however absent from the $C_{10}H_8$ sensitivity spectrum and instead, the reaction between $C_6H_4C_2H$ and C_2H_4 governs the $C_{10}H_8$ formation. As mentioned in kinetic modeling section, this pathway produces an adduct $C_6H_4(CHCH_2)(C\dot{H}CH)$, which subsequently undergoes a ring-closure step forming $C_{10}H_8$ and releasing an H atom. This channel, which skips the formation of naphthyl ($C_{10}H_7$), makes the $C_{10}H_8$ formation mechanism in $C_6H_5C_2H$+C_2H_4 pyrolysis different from those in the other two cases, and results in a significantly higher $C_{10}H_8$ concentrations, owing to the abundant $C_6H_4C_2H$ and C_2H_4 in this reaction system. Besides, C_2H_4 serves as a H atom donator, transforming $C_{10}H_7$ into $C_{10}H_8$ through the reaction $C_{10}H_7$+C_2H_4 => $C_{10}H_8$+C_2H_3. Reactions on the channel initiating from C_6H_5+C_6H_6 which leads to $C_{12}H_8$ formation through multiple steps and intermediates such as cyclopenta[*a*]indene (BENZO) [21,49] have effects on $C_{12}H_8$ concentrations in neat $C_6H_5C_2H$ and $C_2H_5C_2H$+C_2H_4 pyrolysis. These reactions play an important role in the $C_{12}H_8$ formation in benzene pyrolysis, as discussed in our recent work [26]. Although plentiful C_6H_5 and C_6H_6 exist in the currently investigated reaction systems, $C_{12}H_8$ formation is dominated by a more efficient pathway through the HACA route $C_6H_4C_2H$ → $C_{10}H_7$ (or C_9H_6CH) → $C_{12}H_8$ with the addition of two C_2H_2 molecules. In neat $C_6H_5C_2H$ pyrolysis and $C_6H_5C_2H$+C_2H_4 pyrolysis, the reactions controlling C_2H_2 formation, *i.e.* C_6H_5+C_2H_2 = $C_6H_5C_2H$+H and C_2H_4(+M) = H_2CC+H_2(+M), respectively, have positive effects on $C_{12}H_8$ formation. In $C_6H_5C_2H$+C_2H_2 pyrolysis, C_2H_2 already exists as a fuel component, reactions producing $C_6H_4C_2H$ become critical steps. The formation of 1-ethynylnaphthalene ($C_{10}H_7C_2H$) follows the same pathway with that of $C_{12}H_8$, thus showing a negative sensitivity to $C_{12}H_8$ concentration because of the competition. The remarkable difference among the concentration profiles of $C_6H_5CCC_6H_5$ in the three investigated cases is that at the temperature around 1400 K, the concentrations in the pyrolysis of $C_6H_5C_2H/C_2H_x$ are approaching their peaks while that in the case of neat $C_6H_5C_2H$ continue increasing. Results of sensitivity analyses for $C_6H_5CCC_6H_5$ at T_5 = 1400 K are provided

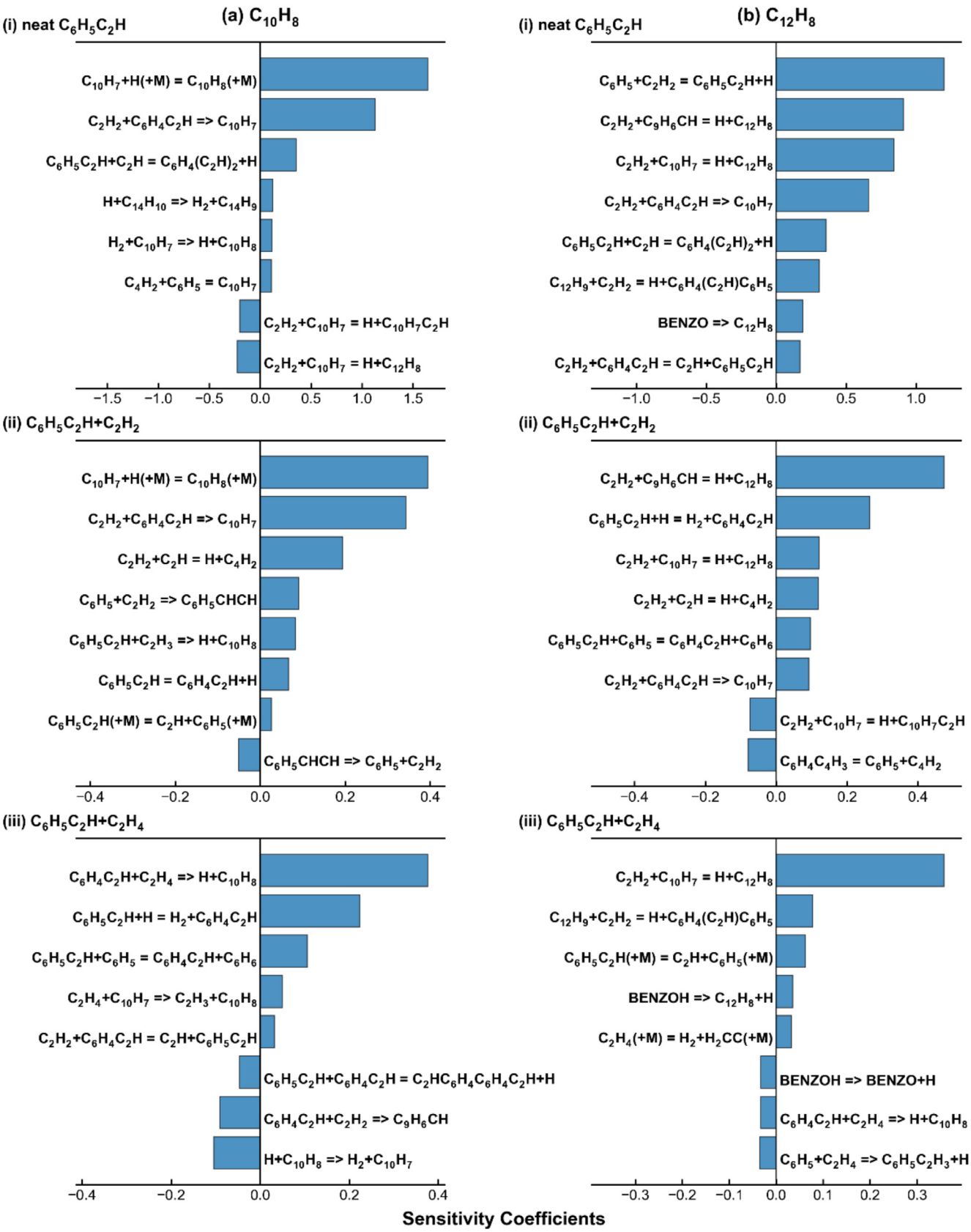

Fig. 11. Sensitivity-analyzed results for (a) $C_{10}H_8$ and (b) $C_{12}H_8$ at T_5 = 1500 K in the pyrolysis of neat $C_6H_5C_2H$, $C_6H_5C_2H+C_2H_2$ and $C_6H_5C_2H+C_2H_4$.

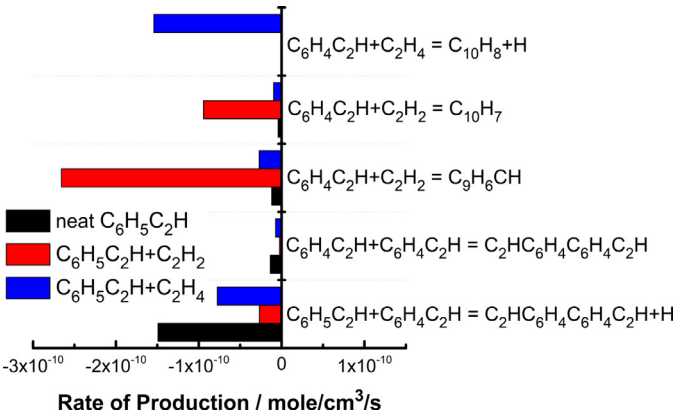

Fig. 12. ROP-analyzed results for $C_6H_4C_2H$ in the pyrolysis of neat $C_6H_5C_2H$, $C_6H_5C_2H$+C_2H_2 and $C_6H_5C_2H$+C_2H_4 mixtures at T_5 = 1380 K.

in Fig. S7(a) in the Supplemental Material. In all three cases, C_6H_5+C_2H_2 = $C_6H_5C_2H$+H (R2), the dominant reaction producing C_6H_5, and $C_6H_5C_2H$+C_6H_5 = $C_6H_5CCC_6H_5$+H (R11), the reaction responsible for $C_6H_5CCC_6H_5$ formation, have high positive sensitivity coefficients. The differences lie in the reactions with negative sensitivity coefficients: in neat $C_6H_5C_2H$ pyrolysis, competitions come from other exiting channels of the $C_6H_5C_2H$+C_6H_5 reactions, including the hydrogen abstraction and the addition-eliminations leading to other $C_{14}H_{10}$ isomers; while in the other two cases, the added C_2 hydrocarbons compete with $C_6H_5C_2H$ to react with C_6H_5, thus inhibiting the formation of $C_6H_5CCC_6H_5$. Different from the cases of $C_6H_5CCC_6H_5$ and $C_{13}H_8CH_2$, the formation of the other $C_{14}H_{10}$ isomer, phenanthrene ($PC_{14}H_{10}$) is not impeded when C_2H_x is added to the reaction system of phenylacetylene pyrolysis, and instead, an obvious increase shows in the peak $PC_{14}H_{10}$ concentration in $C_6H_5C_2H$+C_2H_4 pyrolysis. Sensitivity-analyzed results for $PC_{14}H_{10}$ at T_5 = 1500 K, around which the $PC_{14}H_{10}$ concentrations peak in all three cases, are shown in Fig. S7(b). The most crucial reaction facilitating $PC_{14}H_{10}$ formation is the H-assisted isomerization from $C_6H_5CCC_6H_5$ to $PC_{14}H_{10}$ in each case. The C_2H_4 addition enhances the level of H atoms, and thus the peak concentration of $PC_{14}H_{10}$.

The influences on PAH formation are also reflected by the varying fate of $C_6H_4C_2H$ if a large amount of C_2H_2 or C_2H_4 is present at the initial stage of $C_6H_5C_2H$ decomposition. The ROP analyzed results of $C_6H_4C_2H$ at T_5 of 1380 K, corresponding to that in Fig. S6(a), in the three cases are shown in Fig. 12. In the neat $C_6H_5C_2H$ pyrolysis, $C_6H_4C_2H$ predominantly goes through the addition/elimination reaction with $C_6H_5C_2H$ producing $C_2HC_6H_4C_6H_4C_2H$+H, as detailed previously. This reaction is still partly responsible for $C_6H_4C_2H$ consumption in the cases of $C_6H_5C_2H$+C_2H_2 and $C_6H_5C_2H$+C_2H_4 pyrolysis, but its role is overwhelmed by other channels. HACA routes through $C_6H_4C_2H$+C_2H_2 become important even at relatively low temperatures where the formation of $C_6H_4C_2H$ just begins, if there is abundant C_2H_2 in the reaction system. The resulting C_9H_6CH and $C_{10}H_7$ radicals continue reacting with the ubiquitous C_2H_2 to produce $C_{12}H_8$, as well as a "side product" $C_{10}H_7C_2H$. C_2H_4 in the initial fuel mixture also slightly contributes to the formation of C_2H_2 at the analyzed temperature of 1380 K, so the production of $C_{12}H_8$ and $C_{10}H_7C_2H$ is likewise promoted, but to a lesser extent, for the $C_6H_5C_2H$+C_2H_4 mixtures. But more importantly, C_2H_4 can react with $C_6H_4C_2H$ leading to the formation of $C_{10}H_8$ without the participation of H atoms. The H atoms generated from C_2H_4 decomposition can also aid in the formation of PAH species by promoting formation of the corresponding radical precursors or via H assisted isomerization reactions. For example, $PC_{14}H_{10}$ formation through both $C_{14}H_9$+H and the $C_{13}H_8C_2H$ isomerization increases in the pyrolysis of $C_6H_5C_2H$+C_2H_4. This explains the higher peak concentration of $PC_{14}H_{10}$ even though it is predominantly produced from fuel related pathways of $C_6H_5C_2H$+C_6H_5.

5. Conclusions

A shock tube study was carried out, assisted by kinetic modeling efforts, to investigate the consumption scheme of $C_6H_5C_2H$ under high-pressure pyrolysis conditions, as well as the interactions between the resulting species pool and C_2H_2 (or C_2H_4). Neat $C_6H_5C_2H$ and binary blends of $C_6H_5C_2H$ and C_2H_2 (or C_2H_4) were separately pyrolyzed behind single-pulse shock waves under highly argon-diluted conditions, at the nominal pressure of 20 bar over the temperature range of 1100–1700 K. The experiments reveal the temperature evolution of product formation, including PAH species. In all the investigated cases, the decomposition of $C_6H_5C_2H$ is initiated by C–H bond fission from the aromatic ring. Subsequently, the bimolecular reaction $C_6H_5C_2H$+H = C_6H_5+C_2H_2 dominates the $C_6H_5C_2H$ consumption over the entire temperature window. C_6H_5 is thus produced in plentiful amounts, and it combines with $C_6H_5C_2H$, leading to the formation of $C_{14}H_{10}$ species with concurrent release of H atoms through addition/elimination reactions. This regeneration of H atoms as chain carriers maintains the fuel consumption reactivity. The resulting $C_6H_5CCC_6H_5$, $C_{13}H_8CH_2$ and $PC_{14}H_{10}$ are among the most abundant PAHs in the species pool. The major PAH species produced from $C_6H_5C_2H$ pyrolysis also include acenaphthylene ($C_{12}H_8$), which is formed through HACA routes at relatively high temperatures where C_2H_2 has sufficient concentrations. When extra C_2H_2 or C_2H_4 is introduced to the reaction system, the decomposition of $C_6H_5C_2H$ is negligibly influenced, but the PAH speciation behaviors are altered significantly. In the case of $C_6H_5C_2H$+C_2H_2 pyrolysis, the HACA route through $C_6H_4C_2H$+C_2H_2 starts at low temperatures where $C_6H_4C_2H$ is just produced, giving rise to the remarkable formation of $C_{12}H_8$ from the addition of a second C_2H_2 molecule to the $C_{10}H_7$ radical generated in the first step. In contrast, when a large amount of C_2H_4 is present in the reaction system, considerable $C_{10}H_8$ formation starts early through $C_6H_4C_2H$+C_2H_4. The decomposition of C_2H_4 also contributes to the production of H atoms, facilitating the formation of $C_{10}H_8$ from $C_{10}H_7$. Environments with plenty of C_2H_2 and C_2H_4 result, respectively, in increased formation of acenaphthylene ($C_{12}H_8$) and naphthalene ($C_{10}H_8$), while simultaneously inhibiting the formation of diphenylacetylene ($C_6H_5CCC_6H_5$), which otherwise arises from the competing $C_6H_5C_2H$+C_6H_5 pathways.

Declaration of Competing Interest

The authors declare that they have no known competing financial interests or personal relationships that could have appeared to influence the work reported in this paper.

Acknowledgments

This project has received funding from the European Research Council (ERC) under the European Union's Horizon 2020 research and innovation program (grant agreement No. 756785).

Supplementary materials

Supplementary material associated with this article can be found, in the online version, at doi:10.1016/j.combustflame.2020.06.044.

References

[1] H. Wang, M. Frenklach, A detailed kinetic modeling study of aromatics formation in laminar premixed acetylene and ethylene flames, Combust. Flame 110 (1997) 173–221.
[2] A. Matsugi, A. Miyoshi, Modeling of two-and three-ring aromatics formation in the pyrolysis of toluene, Proc. Combust. Inst. 34 (2013) 269–277.
[3] W. Pejpichestakul, E. Ranzi, M. Pelucchi, A. Frassoldati, A. Cuoci, A. Parente, T. Faravelli, Examination of a soot model in premixed laminar flames at fuel-rich conditions, Proc. Combust. Inst. 37 (2019) 1013–1021.
[4] M. Frenklach, D.W. Clary, W.C. Gardiner Jr, S.E. Stein, Detailed kinetic modeling of soot formation in shock-tube pyrolysis of acetylene, Symp. (Int.) Combust. 20 (1985) 887–901.
[5] M. Frenklach, H. Wang, Detailed modeling of soot particle nucleation and growth, Symp. (Int.) Combust. 23 (1991) 1559–1566.
[6] H. Wang, M. Frenklach, Calculations of rate coefficients for the chemically activated reactions of acetylene with vinylic and aromatic radicals, J. Phys. Chem. 98 (1994) 11465–11489.
[7] J. Appel, H. Bockhorn, M. Frenklach, Kinetic modeling of soot formation with detailed chemistry and physics: laminar premixed flames of C2 hydrocarbons, Combust. Flame 121 (2000) 122–136.
[8] I. Tokmakov, M. Lin, Reaction of phenyl radicals with acetylene: quantum chemical investigation of the mechanism and master equation analysis of the kinetics, J. Am. Chem. Soc. 125 (2003) 11397–11408.
[9] A.M. Mebel, Y. Georgievskii, A.W. Jasper, S.J. Klippenstein, Temperature-and pressure-dependent rate coefficients for the HACA pathways from benzene to naphthalene, Proc. Combust. Inst. 36 (2017) 919–926.
[10] A. Fahr, S.E. Stein, Reactions of vinyl and phenyl radicals with ethyne, ethene and benzene, Symp. (Int.) Combust. 22 (1989) 1023–1029.
[11] E. Heckmann, H. Hippler, J. Troe, High-temperature reactions and thermodynamic properties of phenyl radicals, Symp. (Int.) Combust. 26 (1996) 543–550.
[12] J. Herzler, P. Frank, High temperature reactions of phenylacetylene, Ber. Bunsenges. Phys. Chem. 96 (1992) 1333–1338.
[13] W. Yuan, Y. Li, P. Dagaut, J. Yang, F. Qi, Investigation on the pyrolysis and oxidation of toluene over a wide range conditions. II. A comprehensive kinetic modeling study, Combust. Flame 162 (2015) 22–40.
[14] W. Yuan, Y. Li, P. Dagaut, J. Yang, F. Qi, Experimental and kinetic modeling study of styrene combustion, Combust. Flame 162 (2015) 1868–1883.
[15] W. Yuan, Y. Li, G. Pengloan, C. Togbé, P. Dagaut, F. Qi, A comprehensive experimental and kinetic modeling study of ethylbenzene combustion, Combust. Flame 166 (2016) 255–265.
[16] A. Comandini, G. Pengloan, S. Abid, N. Chaumeix, Experimental and modeling study of styrene oxidation in spherical reactor and shock tube, Combust. Flame 173 (2016) 425–440.
[17] R.A. Tesner, S. Shurupov, Soot formation from acetylene-benzene mixture, Combust. Sci. Technol. 92 (1993) 61–67.
[18] H. Böhm, H. Jander, PAH formation in acetylene–benzene pyrolysis, Phys. Chem. Chem. Phys. 1 (1999) 3775–3781.
[19] A.D. Abid, E.D. Tolmachoff, D.J. Phares, H. Wang, Y. Liu, A. Laskin, Size distribution and morphology of nascent soot in premixed ethylene flames with and without benzene doping, Proc. Combust. Inst. 32 (2009) 681–688.
[20] C.A. Echavarria, A.F. Sarofim, J.S. Lighty, A. D'Anna, Evolution of soot size distribution in premixed ethylene/air and ethylene/benzene/air flames: experimental and modeling study, Combust. Flame 158 (2011) 98–104.
[21] A. Comandini, T. Malewicki, K. Brezinsky, Chemistry of polycyclic aromatic hydrocarbons formation from phenyl radical pyrolysis and reaction of phenyl and acetylene, J. Phys. Chem. A 116 (2012) 2409–2434.
[22] B. Shukla, A. Susa, A. Miyoshi, M. Koshi, In situ direct sampling mass spectrometric study on formation of polycyclic aromatic hydrocarbons in toluene pyrolysis, J. Phys. Chem. A 111 (2007) 8308–8324.
[23] S.J. Harris, A.M. Weiner, Soot particle growth in premixed toluene/ethylene flames, Combust. Sci. Technol. 38 (1984) 75–87.
[24] H. Wang, R. Xu, K. Wang, C.T. Bowman, R.K. Hanson, D.F. Davidson, K. Brezinsky, F.N. Egolfopoulos, A physics-based approach to modeling real-fuel combustion chemistry – I. Evidence from experiments, and thermodynamic, chemical kinetic and statistical considerations, Combust. Flame 193 (2018) 502–519.
[25] R. Xu, K. Wang, S. Banerjee, J. Shao, T. Parise, Y. Zhu, S. Wang, A. Movaghar, D.J. Lee, R. Zhao, A physics-based approach to modeling real-fuel combustion chemistry–II. Reaction kinetic models of jet and rocket fuels, Combust. Flame 193 (2018) 520–537.
[26] W. Sun, A. Hamadi, S. Abid, N. Chaumeix, A. Comandini, Probing PAH formation chemical kinetics from benzene and toluene pyrolysis in a single-pulse shock tube, Proc. Combust. Inst. 38 (2020) Accepted.
[27] D. Nativel, B. Shu, J. Herzler, M. Fikri, C. Schulz, Shock-tube study of methane pyrolysis in the context of energy-storage processes, Proc. Combust. Inst. 37 (2019) 197–204.
[28] A. Comandini, T. Malewicki, K. Brezinsky, Online and offline experimental techniques for polycyclic aromatic hydrocarbons recovery and measurement, Rev. Sci. Instrum. 83 (2012) 034101.
[29] G.P. Wood, L. Radom, G.A. Petersson, E.C. Barnes, M.J. Frisch, J.A. Montgomery Jr, A restricted-open-shell complete-basis-set model chemistry, J. Chem. Phys. 125 (2006) 094106.
[30] J.A. Montgomery Jr, M.J. Frisch, J.W. Ochterski, G.A. Petersson, A complete basis set model chemistry. VI. Use of density functional geometries and frequencies, J. Chem. Phys. 110 (1999) 2822–2827.
[31] Y.-R. Luo, Handbook of bond dissociation energies in organic compounds, CRC Press, 2002.
[32] R. Sivaramakrishnan, K. Brezinsky, H. Vasudevan, R. Tranter, A shock-tube study of the high-pressure thermal decomposition of benzene, Combust. Sci. Technol. 178 (2006) 285–305.
[33] NIST Chemical Kinetics Database, Standard Reference Database 17, Version 7.0 (Web Version), Release 1.6.8, Data Version 2015.09 2015.
[34] A. Matsugi, A. Miyoshi, Reactions of o-benzyne with propargyl and benzyl radicals: potential sources of polycyclic aromatic hydrocarbons in combustion, Phys. Chem. Chem. Phys. 14 (2012) 9722–9728.
[35] J. Park, S. Burova, A. Rodgers, M. Lin, Experimental and theoretical studies of the C6H5+ C6H6 reaction, J. Phys. Chem. A 103 (1999) 9036–9041.
[36] R.S. Tranter, S.J. Klippenstein, L.B. Harding, B.R. Giri, X. Yang, J.H. Kiefer, Experimental and theoretical investigation of the self-reaction of phenyl radicals, J. Phys. Chem. A 114 (2010) 8240–8261.
[37] H. Wang, X. You, A.V. Joshi, S.G. Davis, A. Laskin, F. Egolfopoulos, C.K. Law, Version II, USC Mech. High-temperature Combustion Reaction Model of H2. Reaction Model of H2/CO/C1-C4 Compounds. http://ignis.usc.edu/USC_Mech_II.htm, May 2007.
[38] K. Raghavachari, M.J. Frisch, J.A. Pople, P.v.R. Schleyer, The ground-state singlet potential surface for C2H4, Chem. Phys. Lett. 85 (1982) 145–149.
[39] J.H. Jensen, K. Morokuma, M.S. Gordon, Pathways for H2 elimination from ethylene: a theoretical study, J. Chem. Phys. 100 (1994) 1981–1987.
[40] D. Baulch, C. Cobos, R. Cox, P. Frank, G. Hayman, T. Just, J. Kerr, T. Murrells, M. Pilling, J. Troe, Evaluated kinetic data for combustion modeling. Supplement I, J. Phys. Chem. Ref. Data 23 (1994) 847–848.
[41] I. Tokmakov, M. Lin, Combined quantum chemical/RRKM-ME computational study of the phenyl+ ethylene, vinyl+ benzene, and H+ styrene reactions, J. Phys. Chem. A 108 (2004) 9697–9714.
[42] J. Bittner, J. Howard, Composition profiles and reaction mechanisms in a near-sooting premixed benzene/oxygen/argon flame, Symp. (Int.) Combust. 18 (1981) 1105–1116.
[43] M. Frenklach, N.W. Moriarty, N.J. Brown, Hydrogen migration in polyaromatic growth, Symp. (Int.) Combust. 27 (1998) 1655–1661.
[44] COSILAB, The combustion simulation laboratory, Rotexo GmbH & Co., KG, Haan, Germany, 2009 Version 3.3.2..
[45] W. Tang, K. Brezinsky, Chemical kinetic simulations behind reflected shock waves, Int. J. Chem. Kinet. 38 (2006) 75–97.
[46] X. Han, J.M. Mehta, K. Brezinsky, Temperature approximations in chemical kinetics studies using single pulse shock tubes, Combust. Flame 209 (2019) 1–12.
[47] J.A. Manion, D.A. Sheen, I.A. Awan, Evaluated kinetics of the reactions of H and CH3 with n-alkanes: experiments with n-butane and a combustion model reaction network analysis, J. Phys. Chem. A 119 (2015) 7637–7658.
[48] L.A. Mertens, I.A. Awan, D.A. Sheen, J.A. Manion, Evaluated site-specific rate constants for reaction of isobutane with H and CH3: shock tube experiments combined with bayesian model optimization, J. Phys. Chem. A 122 (2018) 9518–9541.
[49] B. Shukla, K. Tsuchiya, M. Koshi, Novel products from C6H5+ C6H6/C6H5 reactions, J. Phys. Chem. A 115 (2011) 5284–5293.